Assessment of finite volume modeling approaches for intermediate temperature Solid Oxide Fuel Cells working with CO-rich syngas fuels

V. Spallina [a,*], L. Mastropasqua [b], P. Iora [c], M.C. Romano [b], S. Campanari [b]

[a] Chemical Process Intensification, Department of Chemical and Chemical Engineering, Technische Universiteit of Eindhoven, De Random 70, 5612 AP Eindhoven, The Netherlands
[b] Group of Energy Conversion Systems, Department of Energy, Politecnico di Milano, Via Lambruschini 4, 20156 Milano, Italy
[c] Department of Mechanical and Industrial Engineering, Università degli Studi di Brescia, P.zza del Mercato 15, 25121 Brescia, Italy

Received 8 June 2015 Received in revised form 24 August 2015
Accepted 26 August 2015

Abbreviations: SOFC, Solid Oxide Fuel Cell; HT-SOFC, High-temperature SOFC; IT-SOFC, Intermediate-temperature SOFC; DIR, direct internal reforming; SMR, steam methane reforming; WGS, water gas shift; YSZ, yttria-stabilized zirconia; SNG, synthetic natural gas; TPB, triple phase boundary; SS, solid structure.

* *Corresponding author*. Tel.: +31 40 247 8030.
E-mail address: v.spallina@tue.nl (V. Spallina).

Nomenclature

A_{el}	pre-exponential factor, –
$D_{i,j}$	mutual diffusion coefficient of specie *i* into *j*, $m^2\ s^{-1}$
E	activation energy, kJ mol^{-1}
E_{rev}	Nernst ideal potential, V
F	Faraday's constant, C mol^{-1}
h	molar enthalpy, J mol^{-1}
i	current density, A m^{-2}
i_0	exchange current density, A m^{-2}
K_{EQ}	equilibrium constant, –
k_r^-	forward reaction rate constant
k_r^+	backward reaction rate constant
n_e	number of charges transferred in electrochemical process, –
$\dot{N}_i$	molar flow rate of component *i*, mol s^{-1}
p_i	partial pressure of component *i*, Pa
R	ideal gas constant, J $mol^{-1}\ K^{-1}$
R_{TOT}	total electric resistance, Ω
S/C	steam-to-carbon ratio
T	temperature, K
U_f	fuel utilization factor, %
V_{cell}	useful cell voltage, V
x_i	molar fraction, %
ΔG^0	standard reaction Gibb's free energy, kJ mol^{-1}
ΔH^0	Standard reaction enthalpy kJ mol^{-1}

Greek symbols

α_{boud}	coefficient for Boudouard reaction, –
α_{crack}	coefficient for methane cracking reaction, –
β_i	partial pressure order of component *i*, –
η	cell overpotential, V
κ	thermal conductivity, W $m^{-1}\ K^{-1}$
λ	convection heat transfer coefficient, W $m^{-2}\ K^{-1}$
ρ	resistivity, Ω m

Introduction

Solid Oxide Fuel Cells (SOFCs) are energy conversion devices that produce electricity and heat directly from gaseous fuels through an electrochemical oxidation process. SOFCs are expected to play an important role in future power generation due to their high fuel-to-electricity conversion efficiency, both as stand-alone units and particularly in case of integration with thermodynamic cycles [1]. The use of SOFC is also very promising for CO_2 capture applications because this type of fuel cell acts as oxygen separator and thus produces a CO_2 rich-stream at the anode outlet [2–5].

With respect to classic high temperature SOFCs (HT-SOFCs) that operate at 1000 °C, fuel cells at intermediate temperature (IT) working at around 700–800 °C allow using a wider range of materials and a more cost-effective fabrication. IT-SOFCs are generally electrode supported (most frequently anode supported) in order to minimize electrolyte ohmic losses. A typical SOFC electrolyte is yttria-stabilized zirconia (YSZ), while the anode electrode is usually a nickel/zirconia cermet, which provides high electrochemical performance and allows to carry out fuel conversion and oxidation in the same process; the cathode electrode is a perovskite material, such as strontium doped lanthanum manganite (LSM).

The working temperature of IT-SOFCs allows an efficient conversion of gaseous hydrocarbons, such as methane, directly at the anode side (direct internal reforming, DIR) making the operation with natural gas, biogas and other methane-rich syngas fuels very efficient. Additionally, SOFCs are perfectly suited to work with $H_2 - CO$ syngas fuels produced by gasification processes using fossil or renewable solid feedstock. The continuous consumption of H_2 increases CH_4 and CO conversion and the equilibrium of steam methane reforming (SMR) and Water Gas Shift (WGS) reactions moves towards a complete hydrocarbon conversion. Steam-to-carbon ratios are kept high enough to avoid carbon deposition at the anode and subsequent electro-catalyst deactivation and to promote SMR reaction.

The analysis of SOFC power plant performances often requires a detailed simulation of SOFC internal behaviour, both for the development of new cell design and materials and for the investigation of different operating conditions such as fuel composition, temperature and pressure, as well as for optimizing the power plant performances.

The work presented in this paper is based on a previously developed finite-volume model for SOFC simulation [6], updated for a kinetic representations of SMR and WGS reactions and including a detailed electrochemical model for the cases of (i) only H_2 oxidation or (ii) combined H_2–CO oxidation. In particular we focus on the issues related to the use of syngas fuels, like those generated by coal or biomass gasification. These processes often feature high CO and/or CH_4 contents depending on the gasification technology and on the type of integration with the power cycle (see for instance the proposals for high CO gasification in Romano et al. [7] as well as the studies on catalytic gasification [8] or about the use of methanation reactors in [9]).

A literature review of the existing SOFC models is firstly presented to introduce the different approaches with particular attention to the kinetic and the electro-chemical models adopted. Then we discuss the kinetic and electrochemical model, which allows calculating the material and energy balances, considering the cases of either H_2-only or H_2–CO oxidation. Validation of the relevant model parameters is based on a wide set of literature data that refers to both HT-SOFC and IT-SOFCs.

The results of the SOFC simulation tool are finally compared with other literature models. With reference to a co-flow cell configuration, different aspects are commented and highlighted, especially focusing on the effects of the operating pressure and of the inlet feed composition. In particular, the assessment of the modeling importance of the combined electrochemical oxidation of H_2 and CO is performed for different inlet fuel compositions. The results ought to provide a modeling aid as in which working conditions and with which inlet composition a simpler model might be used, yet with only a negligible loss in the performance prediction accuracy.

The work includes a sensitivity analysis on the activation energy at both anode and cathode electrodes, as well as an analysis of the relative proportion of H_2 and CO-related

current densities depending on the inlet fuel composition. Finally, a thermodynamic analysis is carried out to evaluate the risk of carbon deposition, according to Boudouard and methane cracking reactions. Although several SOFC models have been presented and proposed in literature, most of them discuss the performance of a single system and often the analysis is then extended to different operating conditions. These aspects were developed as deeply correlated to the nature of the inlet fuel composition by studying SOFCs fed with syngas fuels such as those generated in coal-based or biomass gasification power plants.

Literature review of SOFC models

Several works have been presented in literature about SOFC modeling, adopting different approaches to describe the reaction kinetics and the electrochemical behaviour of these fuel cells; below we summarize the main features of some of the outstanding ones.

Kinetic model approaches to SMR and WGS

SOFCs can be very efficient in performing hydrocarbon-based fuel conversion. Due to the tolerance to CO and CO_2, they can operate directly with natural gas or syngas, suppressing the external process of fuel conversion into H_2-rich stream, which is typically required by low temperature fuel cells (e.g. based on PEMFC, AFC, etc.). The heat released by the electrochemical process is exploited to drive endothermic catalytic reforming reactions; this feature gives SOFCs an undisputable advantage in terms of fuel flexibility. The global reactions mechanism involved generally includes the steam methane reforming reaction (SMR, E 1) in presence of humidified CH_4-rich syngas and the Water Gas Shift reaction (WGS E 2).

$$CH_4 + H_2O \underset{k_r^-}{\overset{k_r^+}{\leftrightarrows}} 3H_2 + CO \quad \Delta H^0(kJ/mol) = 206 \qquad \text{E1}$$

$$CO + H_2O \underset{k_w^-}{\overset{k_w^+}{\leftrightarrows}} H_2 + CO_2 \quad \Delta H^0(kJ/mol) = -41.6 \qquad \text{E2}$$

where k_r^+, k_w^+ and k_r^- *e* k_w^- represent the forward and reverse reaction kinetic constants, respectively for SMR(r) and WGS(w). The majority of literature models deal with natural gas applications and the most widely used functions for the kinetic constants are summarized in Table 1 and Table 2. Among those, Aguiar et al. [10] describe a mathematical model of YSZ electrolyte 1-D co-flow and counter-flow SOFC

Table 1 – List of different models used for the kinetic of the SMR reaction.

Equation for SMR in anode-SOFC	References
$\frac{d\dot{N}_{CH_4}}{dt} = k_r^+(p_{CH_4} \times p_{H_2O}) - k_r^-(p_{CO} \times p_{H_2}^3)$	[15–18]
$\frac{d\dot{N}_{CH_4}}{dt} = K_R(p_{CH_4}^{\beta_1} \times p_{H_2O}^{\beta_2}) \times e^{\frac{-E_{CH_4}}{RT}}$*	[10,13,14]
$\frac{d\dot{N}_{CH_4}}{dt} = K_R(p_{CH_4}^{\beta_1} \times p_{H_2O}^{\beta_2}) \times e^{\frac{-E_{CH_4}}{RT}} \times D_a$*	[19]

(*) β_1, β_1,k_0, E_{CH4} vary from study to study according to authors assumptions and anode-SOFC operating conditions.

Table 2 – List of different models used for the kinetic model of the WGS reaction.

Equation for SMR in anode-SOFC	References
$\frac{d\dot{N}_{CO}}{dt} = k_o^{WGS} \times p_{CO} \times \left(1 - \frac{(p_{CO_2} \times p_{H_2})}{(p_{CO} \times p_{H_2O}) \times K_{WGS}}\right)$ $K_{WGS} = e^{\frac{4276}{T(K)} - 3.961}$	[15–18]
$\frac{d\dot{N}_{CO}}{dt} = k_w^+(p_{CO} \times p_{H_2O}) - k_r^-(p_{CO_2} \times p_{H_2})$	[10,13,14]

operating with pre-reformed natural gas with direct internal reforming, working at atmospheric pressure and temperature in the range of 700–800 °C. The model used for the mass balance assumes that all the CH_4 is converted through the SMR reaction by assuming a first order kinetic expression that depends on reactants partial pressures, while WGS is considered at the equilibrium. The effect of H_2O and CH_4 partial pressures is accounted for with different coefficients according to the operating parameters of the system. The same kinetic model for SMR and WGS has been used also in Campanari and Iora [6] both in a 2D planar model for SOFC fed by pre-reformed natural gas at atmospheric pressure and operating temperature of 1000 °C, as well as in a tubular configuration at atmospheric and pressurized conditions [11]. The CH_4 conversion is calculated with a kinetic approach that takes into account the partial pressure of CH_4 according to the original work of Achenbach et al. [12], Costamagna et al. [13], while the WGS reaction is calculated at equilibrium. The same model is also used in Li et al. [14]. The use of pressurized SOFC and different syngas composition is discussed in Gemmen et al. [15] which specifically focuses on the use of coal-derived syngas in SOFCs based on planar Ni/YSZ cermet. The model provides the description of the transport of gases through the anode, as well as gas species reactions within the anode. The chemical reactions are calculated according to Lenhert et al. [16], Habermann and Young [17] and Divisek et al. [18] by introducing forward and reverse rate constants for the two reactions. Results show the effect of pressure on the SMR reaction; in particular, at high pressure the H_2 is consumed to form CH_4, which partly counterbalances the effect of steam formation.

Yakabe et al. [19] proposed a 3D mathematical model for a planar SOFC operating at 900–1000 °C. Different input parameters have been used for the simulation such as fuel velocity, flow pattern and syngas composition. The rate of CH_4 conversion via SMR is calculated adopting an empirical formula for Ni/YSZ in an Arrhenius form that depends on reactants partial pressure and anode structure density (D_a), while WGS rate of conversion is determined from the forward and backward reactions.

As an alternative approach to global reforming models, more detailed reaction mechanisms have also been proposed in the open literature. The most recent and reliable one is that proposed by Janardhanan et al., 2006 [20] (the complete model shall also be found at www.detchem.com/mechanisms), based upon 42 irreversible reactions comprising 6 gas-phase species and 12 surface adsorbed species. It extends the model already presented by Hecht et al., 2005 [21] to a wider temperature range (220–1700 °C). Most of the considered

reactions kinetics are expressed as Arrhenius-like equations taking into account the heterogeneity nature of the chemical process. The authors report an assessment the carbon deposition, electrochemical cell overpotentials and transport mechanisms with respect to H_2O content, current density, catalyst coverage of adsorbed species and operating temperature.

Unfortunately, much uncertainty is still present among SOFC researchers about the reliability of either global or detailed reforming reaction models. Hoffman et al., 2009 [22] propose a comparison of the two approaches: a global model extensively cited in the SOFC modeling open literature (Achenbach et al., 1994 [12]) and the more recent previously described elementary heterogeneous chemical kinetics model proposed by Janardhanan et al., 2006 [20].

In conclusion, two extremely detailed reviews on SOFC general multi-scale modeling by Andersson et al., 2010 [23] and on internal steam reforming kinetics by Mogensen et al., 2011 [24], report the general trends used to address these issues and the still numerous unresolved areas. They both conclude that it is still urged an exhaustive experimental work which ought to delve into the intimate correlation between kinetics, microstructure and SOFC performance.

The effect of carbon deposition is often discussed in relation to anodic reforming reactions of hydrocarbons as the presence of Ni on the anode surface enhances the carbon formation via Boudouard and methane cracking reactions. The formation of solid carbon has to be prevented to avoid fast degradation of the cell and a relevant cell voltage drop. A comprehensive discussion of the phenom-ena and the effect on cell performance and the strategies to limit carbon formation are reported in Miao et al. [25]; moreover, Klein et al. [26] discussed the effect of syngas composition and current density from a qualitative point of view, with the calculation of the α coefficients for the Boudouard (E4) and methane cracking (E3) reactions, expressed by:

$$CH_4 \leftrightarrow 2H_2 + C \quad \alpha_{crack} = \frac{p_{H_2}^2}{p_{CH_4} K_{crack}} \tag{E3}$$

$$2CO \leftrightarrow C + CO_2 \quad \alpha_{boud} = \frac{p_{CO_2}}{p_{CO}^2 K_{Boud}} \tag{E4}$$

The α coefficients represent the ratio between the driving force to consume solid C (partial pressure reactants ratio) and the chemical equilibrium constant of the reactions involved.

When α_j in equations (E3) and (E4) is higher than 1 the carbon deposition is not thermodynamically possible, while if α_j is lower than 1, a kinetic model is needed to estimate if carbon deposition occurs and consequently its deposition rate.

Electrochemical model approaches

SOFCs operated under open-circuit conditions show a maximum cell voltage $V_{oc,cell}$ close to the reversible one, known as Nernst potential E_{rev}. A difference can arise in presence of internal parasitic currents that short-circuit part of the cell potential even at open circuit. However, these losses are generally small and highly dependent on the cell design and manufacture, consequently, they are usually neglected at a modeling level; by contrast, they can be included when calibrating a model against specific experimental results [27]. If this effect was neglected, it is possible to write:

$$V_{OC,cell} = E_{rev} = -\frac{-\Delta G_r^0}{n_e F} - \frac{RT}{n_e F} \ln \prod p_k^{\upsilon_k} \tag{E5}$$

While the current is delivered, the reversible potential and the open circuit potential cannot be achieved. The electric potential losses are related to internal barriers and are called overpotentials η_i. Three different overpotential or voltage losses are typically distinguished: i) *activation* overpotential, associated to the energy needed to start electrodes kinetically controlled reactions; ii) *ohmic* overpotential, related to the effect of resistivity along the surfaces of electrodes, interconnections and electrolyte associated to the passage of electrons and oxygen ions; iii) *concentration* overpotential, associated to gas-phase transport limitations within the porous electrode structures, which tend to make the gas composition at cell reaction sites different from that in the bulk flow. The final cell voltage is then expressed as:

$$V_{cell} = E_{rev} - \eta_{ohm}(i) - \eta_{act,an}(i) - \eta_{act,cat}(i) - \eta_{conc,an}(i) - \eta_{conc,cat}(i) \tag{E6}$$

Overpotentials modeling

The Ohmic losses are modeled by the first Ohm's law where the equivalent ohmic resistance depends on the anode, cathode and electrolyte resistances, that are generally calculated with the second Ohm's law. Provided the cell geometry and material resistivity as function of temperature, its simulation is mathematically straightforward, as shown in Table 3 for typical SOFC materials.

The concentration overpotentials are related, as already mentioned, to mass transport limitations. An insightful recent review by He et al., 2013 [28] specifically delves into the gas transport mechanisms inside the porous electrodes and the associated main losses which characterise SOFCs operation. In addition, subsequently to a review of diffusion models, an appraisal of diffusivity measurement techniques is performed, experimentally underlying the deep correlations between concentration polarisations and electrode thickness, porosity and tortuosity with respect to temperature and current density design choices.

In particular, a lower reactant concentration at cell reaction sites (TPB) with respect to the bulk flow leads to a voltage loss. Such a loss has always been considered of minor importance compared to other irreversibilities terms; however, due to the increasingly higher values of current density targets, the thorough understanding and modeling of this term has also become crucial.

From a mathematical point of view, the diffusion process inside the porous electrode materials can be calculated using the Knudsen model, which expresses the

Table 3 – Correlations used for the calculation of resistivity of SOFC materials (from Ref. [11]).

Layer	ρ [Ωm]	Material type
Anode	1.25×10^{-5}	Ni-YSZ cermet
Cathode	1.19×10^{-4}	Perovskite materials (i.e. LSM, LSCF)
Electrolyte	$\left(33.4 \times 10^{3} \times e^{\frac{-103000}{T(K)}}\right)^{-1}$	YSZ
Interconnect	$\left(\frac{9.3 \times 10^{6}}{T} e^{\frac{-1100}{T(K)}}\right)^{-1}$	Ceramic oxides with perovskite structure (i.e. $LaCrO_3$)

functionality upon the average pore size and tortuosity. Hence, η_{conc} depends on electrodes thickness, porosity and tortuosity and, at a first approximation, it is proportional to the partial pressure of reactant species. The diffusion through porous media in SOFC can be described by adopting three different methods:

- The Fick's Law Model, described in Chan et al. [29], characterises the transport of components through the gas phase and within a porous media and it is commonly used in binary or diluted mixtures. The diffusion coefficient is written combining the molecular diffusion and the Knudsen diffusion coefficient.
- The Stephan–Maxwell Model is commonly used for multicomponent systems: it is used for the calculation of the species fluxes and it is based on the Stephan–Maxwell equations for the gas diffusion. This model is more comprehensive than the Fick's law model because it does not exclude the possibility of negative diffusion coefficients. The analytical solution of the mass transport phenomena equations for the Stephan–Maxwell Model is generally difficult to be found due to the lack of calculated diffusion coefficients for multicomponent systems. The comparison of Fick's Law and Stephan–Maxwell models has been discussed in Suwanwarangkul et al.[30].
- The Dusty Gas Model is an extension of the Stephan–Maxwell Model that takes into account the Knudsen diffusion phenomena and the effect of different molecular weights in the counter diffusion process, which is also assumed in the Fick's Law Model. In the last case the diffusion is described by the following equation, as reported in Yakabe et al. [31].

$$\frac{N_i}{D_{i,k}^{eff}} + \sum_{j=i, j\neq i}^{n} \frac{y_j N_i - y_i N_j}{D_{i,j}^{eff}} = -\frac{p}{RT}\frac{dy_i}{dz} \qquad \text{E7}$$

The prediction of the activation overpotential is generally based on the Butler–Volmer relationship in the implicit form:

$$i = i_0 \left[\exp\left(\frac{n_e \eta_{act,el} F}{RT}\alpha\right) - \exp\left(\frac{n_e \eta_{act,el} F}{RT}(\alpha - 1)\right)\right] \qquad \text{E8}$$

where subscript *el* refers either to cathode or anode, α is the transfer coefficient (usually chosen equal to 0.5) and i_0 is the exchange current density to be determined for both the electrodes. At high temperature (e.g. 1000 °C) the electrode reaction is fast with the consequence of small overpotential losses, but when the SOFC operating temperature reduces the activation losses can represent the most relevant voltage loss. A lot of research is ongoing and several works have been published on this topic but a detailed understanding of the electrode reaction mechanism, the relationship with its microstructure and its effects on cell losses is still debated. Aguiar et al. [10] assumed a Butler–Volmer equation correction when considering the anode, because the charge and mass transfer occur at comparable rates; Campanari and Iora [6] calculated the exchange current density i_0 following the values reported in Costamagna et al. [13]. The overpotential is approximated in linear form with respect to the current *i* if the polarization conditions are low, or neglecting the second term in the equation (Table 4) and writing the relation as Tafel's law [32].

The different models usually differ in the definition of i_0. The general equation used for the calculation of the exchange current density is an Arrhenius type equation, dependent on the pre-exponential factor A_{el} and the activation energy E_{el} for both electrodes:

$$i_0 = A_{el} \cdot e^{\frac{-E_{el}}{RT}} \qquad \text{E9}$$

The SOFC models presented in literature use different definitions of the terms A_{el} and E_{el}, resulting in different dependences on temperature, pressure and reactant concentrations as reported in Table 4 for some representative works. The A_{el} and E_{el} differ from case to case because they feature different operating conditions, cell geometries and flow configurations in order to fit the experimental data. Moreover, anticipating here the subject of point 4.3, in presence of H_2–CO combined oxidation it is necessary to separate the activation overpotential for H_2 and CO oxidation, with different coefficients; unfortunately, poor consistency in their definition is present in the literature. A different approach was originally proposed by Achenbach [33] with the use of a simplified method where the activation overpotentials are written in terms of electrical resistances and thus directly calculated as function of the current.

If only H_2 oxidation is assumed, the equivalent electric circuit model is shown in Fig. 1a; the various terms of electrochemical equations and the resulting current flow are related only to H_2 oxidation [10,11,14,26], On the contrary, when direct CO oxidation is considered, the equivalent electric circuit changes into the one shown in Fig. 1b. In the latter case, the resulting electrochemical balance becomes a system of non-linear equations, which can be expressed as follows:

$$\begin{cases} V_{cell} = E_{rev,H_2} - \eta_{ohm}(i) - \eta_{act,H_2}(i_{H_2}) - \eta_{act,cat}(i) - \eta_{conc,H_2}(i_{H_2}) - \eta_{conc,cat}(i) & \text{E 7} \\ V_{cell} = E_{rev,CO} - \eta_{ohm}(i) - \eta_{act,CO}(i_{CO}) - \eta_{act,cat}(i) - \eta_{conc,CO}(i_{CO}) - \eta_{conc,cat}(i) & \text{E 8} \\ i = i_{H_2} + i_{CO} & \text{E 9} \end{cases}$$

where $E_{rev,j}$ is the Nernst potential of reaction j (respectively H_2 and CO oxidation), and i_{H_2} and i_{CO} are the current densities associated to H_2 and CO oxidation. It is worth noting that when the current density tends to zero the system is valid only if the water gas shift reaction is at chemical equilibrium and thus the Nernst potential of CO and H_2 are the same.

The activation overpotential related to CO oxidation can be computed in different ways, and the two most common simulation approaches are the following:

i) the activation overpotentials are calculated as electrical resistances as proposed by Achenbach [33] and also performed in Nishino et al. [34] or Petruzzi [35];
ii) the Butler–Volmer equation is adopted, using different parameters that are calibrated after fitting experimental data. This procedure is generally based on the assumption that the current generated by hydrogen oxidation is higher than the current generated by carbon monoxide oxidation; however, different approaches are possible, ranging from the definition of a constant ratio between the two currents

Table 4 – Correlations found in literature for the calculation of activation overpotentials at anode and cathode sides.

Pre-exponential factor A_{el} [Am^{-2}]		Ref.
Anode	Cathode	
$A_{an,i} = \frac{RT}{n_e F} k_{an}$	$A_{cat} = \frac{RT}{n_e F} k_{cat}$	[10,14,26,46]
$A_{an,i} = \left(\frac{p_{H_2O/CO_2,TPB}}{K_{eq,i}\ p_{H_2/CO,TPB}}\right)^{0.266} \frac{RT}{F} k_{an,i}$ i is the reactions CO to CO_2 or H_2 to H_2O	$A_{cat} = (p_{O_2})^{0.5} \frac{RT}{F} k_{cat}$	[38–40]
$A_{an,i} = k_{an}\left(\frac{p_{H_2/CO}}{p_{amb}}\right)\left(\frac{p_{H_2O/CO_2}}{p_{amb}}\right)^{m}$ i is the reactions CO to CO_2 or H_2 to H_2O	$A_{cat} = k_{cat}\left(\frac{p_{O_2}}{p_{amb}}\right)^{0.25}$	[6,13,47]
Direct calculation of the activation overpotentials		
$\eta_{act,H_2/CO} = i_{H_2/CO}\left(\left(\frac{p_{H_2/CO}}{p_{fuel}}\right)^{0.25} k_{H_2/CO} \frac{2F}{RT} exp\left(-\frac{E_{an}}{RT}\right)\right)^{-1}$	$\eta_{act,O_2} = i\left(\left(\frac{p_{O_2}}{p_{air}}\right)^{0.25} k_{O_2} \frac{4F}{RT} exp\left(-\frac{E_{cat}}{RT}\right)\right)^{-1}$	[33–35]

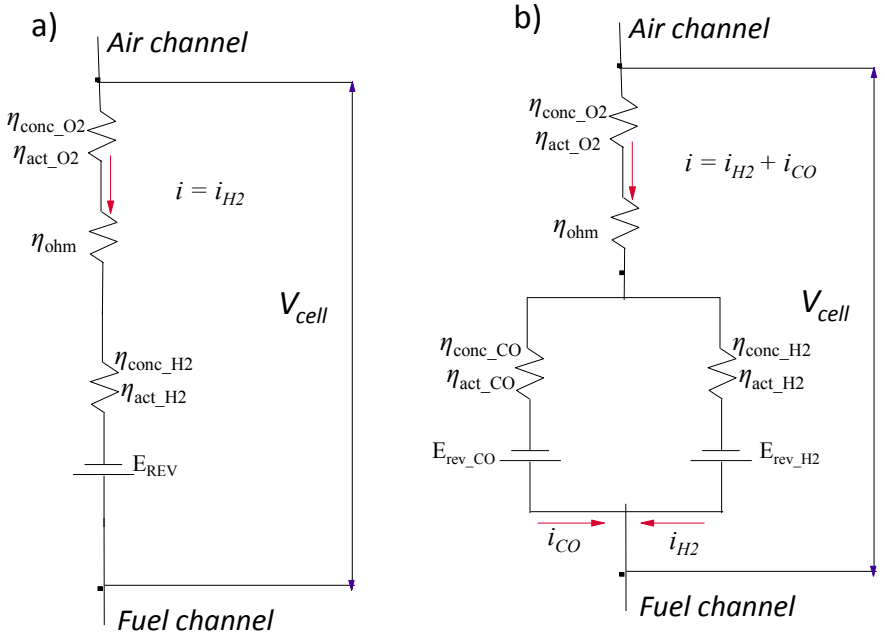

Fig. 1 – Equivalent electric circuit models for the H_2 only oxidation (left) and for the H_2–CO oxidation (right) where two parallel branches for the respective currents i_{CO} and i_{H_2} are highlighted.

to more complicated models. Reflecting this approach, Gemmen et al. [15] assumed that $i_{H_2} = 4 \times i_{CO}$, while Matsuzaki et al. [36] suggested that the ratio between electrochemical oxidation of H_2 and CO is in the range 2.5:3. More recently, Ni 2012 [37] considers $i_{H_2} = 2.5 \times i_{CO}$ for SOFC running on partially pre-reformed gas mixture. In another work, Suwanwarangkul et al. [38] describes a more complete model in which the exchange current density of CO is 2.5 times lower than that of H_2; moreover, the current densities are also dependent on the equilibrium constants respectively of H_2 and CO oxidation. The same model has also been used recently in Andersson et al. [39] and Iwai et al. [40].

A detailed and comprehensive description of the different models is discussed in two exhaustive reviews by Hajimolana et al., 2011 [45] and Kakaç et al., 2007 [46] in which a significant number of references and assumptions are reported. Interestingly, the cited authors overview the topics which still need further research; amongst these, the combined electrochemical oxidation of CO + H_2 is said to be characterised by still unknown proportions of the two reactions at the TPB, leading to a doubtful effect of simplifying assumptions of the electrochemical model upon the accuracy of the performance prediction. Furthermore, SOFC modeling, concerning hydrocarbon-based syngas fuels feeds, suggests the need of additional insights on the effect of fuel composition and its consequences on SOFCs perfor-mance [45]. Similar approaches for planar cells operated in co-current and cross-flow feeding direction in the range of 700–900 °C to the ones here discussed have been presented in the recent years including also the experimental validation [41–44] up to 2 kW.

In conclusion, despite the large amount of SOFC models present in the open literature, a comparison of them, the effects on the SOFC performance using different reaction mechanisms and also comparison of different syngas composition has not been carried out using common assumptions.

Model description

In this work, a previously developed and validated model, reported in Campanari and Iora [6] has been updated, in order to address the specific modeling tasks underlined in Chapter 2. The detailed analysis of the mathematical formalism, including the discretization method and the solution for the equation solver have been described in Campanari and Iora [6]. The cell configuration is limited to planar SOFCs, with different possible designs namely co-flow, counter-flow and cross-flow streams arrangements.

Despite the model is able to simulate different flow configurations, the analysis hereby presented is focused for simplicity on the reference case of a co-flow configuration, represented in Fig. 1. Single cells can be connected to generate more power, given the possibility to create modules that form a SOFC stack (for instance as shown in Fig. 1). However, for the purposes of our discussion we focus here on the simulation of the operating conditions of a generic intermediate cell of the stack, where the interconnections are considered adiabatic. Moreover, thanks to the simplicity of the co-flow arrangement, we will focus on the distribution of thermodynamic variables along a generic intermediate channel within the cell plane, resulting in a 1D perspective.

The specifications of the cell channel considered in the simulations are reported in Table 5. The assumptions are not related to any specific manufacturer's design and are selected to allow comparison with previous literature results. The resulting active area is 400 mm^2, referring to the free electrode surface exposed to reactants.

Any 3D effect dealing with temperature distribution and heat losses along the y-axis could be addressed keeping the same kinetic and electrochemical model, with relatively marginal implications on the accuracy of the 1D-results as already discussed by some of the authors in Iora and Campanari [47].

Kinetic model of SMR and WGS

The kinetic model proposed in Divisek et al. [18] has been selected, which considers the cell operating pressure effects and the dependency upon the partial pressure of both reactants and products; in this way the effect of the fuel feed composition can be addressed. The overall model is arranged to calculate firstly the kinetics of SMR and WGS reactions and then the electrochemical oxidation of H_2 or H_2/CO. For Ni-based material the forward reaction rate constants (k_r^+ *and* k_w^+) of reactions E1 and E2 are described by polynomial equations (E12, E13) and hence SMR (subscript *r*) and WGS (subscript *w*) reactions (R_r and R_w) at three phase boundary (TPB) are described by means of coefficients that describe their kinetics.

The rate constants can be expressed in Arrhenius form throughout the following equations:

$$\frac{d\dot{N}_{CH_4}}{dt}\left[\frac{mol}{m^3 s}\right] = R_r = k_r^+\left(p_{CH_4} \times p_{H_2O}\right) - k_r^-\left(p_{CO} \times p_{H_2}^3\right) \quad \text{E10}$$

$$\frac{d\dot{N}_{CO}}{dt}\left[\frac{mol}{m^3 s}\right] = R_W = k_w^+\left(p_{CO} \times p_{H_2O}\right) - k_w^-\left(p_{CO_2} \times p_{H_2}\right) \quad \text{E11}$$

The forward and backward reaction rate constants are calculated with the set of equations presented below, whereby the rate constants k_r^+ *and* k_w^+ and the equilibrium constants K_{eq}^{SMR}, K_{eq}^{WGS} are a function of temperature and k_r^- *and* k_w^- a function of gas species partial pressures.

$$k_r^+ = (1.942)(2395)exp\left(\frac{-231266}{RT}\right) \quad \text{E12}$$

$$k_w^+ = (1.185)(0.0171)exp\left(\frac{-103191}{RT}\right) \quad \text{E13}$$

Table 5 – Dimensions of the unit cell elements assumed in the simulation.

Cell length, mm	400	Anode thickness, μm	500
Cell width, mm	1	Cathode thickness, μm	50
Fuel channel height, mm	1	Electrolyte thickness, μm	20
Air channel height, mm	1	Interconnect thickness, μm	500

$$K_{eq}^{SMR} = \frac{k_r^+}{k_r^-} = \frac{p_{CO} p_{H_2}^3}{p_{CH_4} p_{H_2O}} \quad \text{E14}$$

$$K_{eq}^{WGS} = \frac{k_w^+}{k_w^-} = \frac{p_{CO_2} p_{H_2}}{p_{CO} p_{H_2O}} \quad \text{E15}$$

$$K_{eq}^{SMR} = (1.003)(1.0267 \times 10^{10}) exp(-0.2531Z^4 + 0.3665Z^3 + 0.581Z^2 - 27.134Z + 3.277) \quad \text{E16}$$

$$K_{eq}^{WGS} = (1.049) exp(-0.2935Z^3 + 0.6351Z^2 + 4.1788Z + 0.3169) \quad \text{E17}$$

$$Z = \frac{1000}{T(K)} - 1 \quad \text{E18}$$

Thus, the resulting molar rates of formation for the various species are:

$$\frac{d\dot{N}_{CH_4}}{dt} = -R_r; \frac{d\dot{N}_{CO}}{dt} = R_r + R_W; \frac{d\dot{N}_{CO_2}}{dt} = R_W; \frac{d\dot{N}_{H_2}}{dt} = 3R_r + R_W; \frac{d\dot{N}_{H_2O}}{dt} = -R_r - R_W$$

It can be noted that by adopting this model: i) WGS is not considered at equilibrium, oppositely to what is proposed by most literature works; ii) in the SMR the effect of pressure is taken into account.

Electrochemical model

As already anticipated in Chapter 2, two different electrochemical models have been implemented. The first considers only the electrochemical conversion of H_2, while the second calculates the current contributions of both H_2 and CO. In the following, we will refer to the two models as "H_2-only"and "H_2–CO" model. The latter has been also studied using reduced activation energies, featuring the performance of an advanced SOFC (named *H_2–CO evo*).

After running the kinetic model, which calculates the composition in a generic cell element (Fig. 2), the electrochemical model calculates the current flow, the power output and solves the mass balance of the system. For all cases, a uniform average temperature of each cell element is assumed for the solid structure, as well as for the anode and the cathode flow.

The correlations used for the models are taken from the literature. In case of the "H_2-only" model, the reference considered is Aguiar et al. [10] while in case "H_2–CO" the model of Suwanwarangkul et al. [38] has been used (properly corrected in the "*H_2–CO evo*" model). The set of equations required for the estimation of the overpotential losses are listed in the next paragraphs and it will include the case with only H_2 oxidation and combined H_2 and CO oxidation.

Nernst voltage

The Nernst voltage is the maximum cell voltage achievable if the current output is zero, defined for H_2 and CO as function of temperature, pressure and reactants composition. Equations E19 E21 represent the Nernst voltages respectively for H_2 and CO oxidation reactions, while equations E20 and E22 are used to calculate the standard potentials as function of solid temperature:

$$E_{rev,\,H_2}(or\ V_{H_2}) = E_0^{H_2} - \frac{RT}{2F} ln\left(\frac{p_{H_2O}}{p_{H_2}\left(p_{O_2}/101325\right)^{0.5}}\right) \quad \text{E19}$$

$$E_0^{H_2} = 1.2729 - (2.7632 \times 10^{-4}) T_{ss} \quad \text{E20}$$

$$E_{rev,\,CO}(or\ V_{CO}) = E_0^{CO} - \frac{RT}{2F} ln\left(\frac{p_{CO}}{p_{CO}\left(p_{O_2}/101325\right)^{0.5}}\right) \quad \text{E21}$$

$$E_0^{CO} = 1.4671 - (4.5292 \times 10^{-4}) T_{ss} \quad \text{E22}$$

Ohmic overpotential

Ohmic losses are caused by the resistance to conduction of ions and electrons through the cell components. The overall system resistance is divided amongst the losses in the air channel interconnection, in the solid structure (SS) composed by anode, cathode and electrolyte layers and in the fuel channel interconnection.

The solid structure resistance (Fig. 3a) is calculated from the temperature-dependent material resistivity of anode, cathode and electrolyte, considering the equivalent electric circuit shown in Fig. 3b, following the approach proposed in Campanari and Iora [11]. The resistance of the interconnections is calculated considering to divide the "L-shaped" structure of Fig. 3a into three rectangular parts (I, II, III); the resistances are computed by means of the Ohm's law (the resistance of the element III R_{III} is calculated using an empirical function), where the material resistivity is calculated according to the correlations listed in Table 3.

$$R_{ss} = \frac{\sum_{k=an,cat,el} \rho_k \delta_k}{A} \quad \text{E23}$$

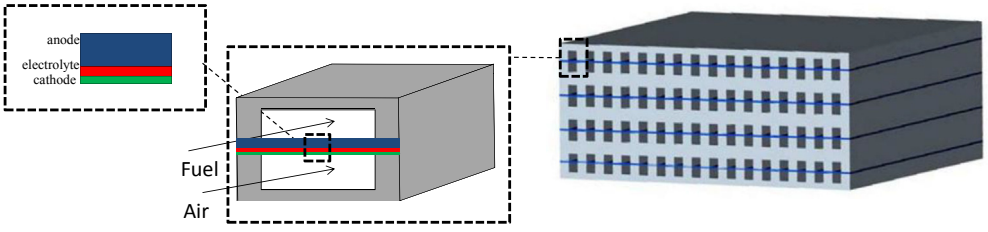

Fig. 2 – Unit cell element in co-flow configuration (left) and SOFC stack (right).

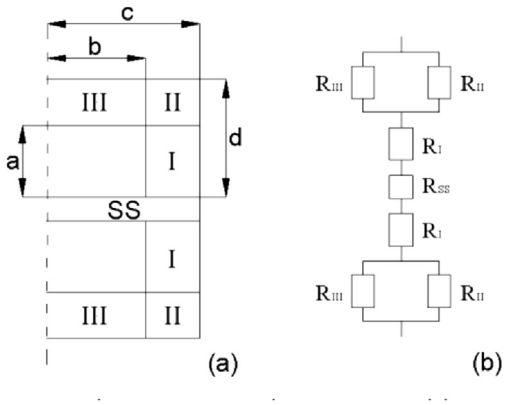

Fig. 3 – Ohmic overpotential geometric model (a), and equivalent electric circuit (b) for one cell element of length equal to "z" with a solid structure (SS) thickness equal to "δ".

$$R_I = \frac{a\rho_{ic}}{z(c-b)};\ R_{II} = \frac{(d-a)\rho_{ic}}{z(c-b)};\ R_{III} = \frac{\rho_{ic}}{z}\frac{1}{0.41\left[1-exp\left(-1.2\frac{b}{d-a}\right)\right]} \quad \text{E24}$$

$$R_{TOT} = \frac{R_{III}R_{II}}{R_{III}+R_{II}} + R_I + \frac{R_{SS}}{2} \quad \text{E25}$$

$$\eta_{ohm} = R_{TOT}\, i \quad \text{E26}$$

Concentration overpotential

Concentration overpotentials η_{conc} are function of the current density; in particular, at increasing current, the fuel consumption rate rises, leading to a faster decrease of the reactants partial pressure at the reaction sites (TPB), whilst the production rate of the products increases. The presence of reactions in the porous anode while the reactants are diffusing is not considered in the present model, therefore the CO, H_2 are decreasing monotonously from the bulk to the TPB. However, due to the low contribution of the concentration overpotential to the cell voltage the expected results do not change significantly and a more detailed diffusion model will be implemented in a future work.

The expressions used to evaluate η_{conc} at anode and cathode side are listed below, depending on the concentrations at TPB and in the bulk flow:

$$\eta_{conc,\,cat} = \frac{RT_{ss}}{4F} ln\ \left(\frac{x_{O_2}^{bulk}}{x_{O_2}^{TPB}}\right) \quad \text{E27}$$

$$\eta_{conc,\,H_2} = \frac{RT_{ss}}{2F} ln\left[\left(\frac{x_{H_2}^{bulk}}{x_{H_2}^{TPB}}\right)\left(\frac{x_{H_2O}^{bulk}}{x_{H_2O}^{TPB}}\right)\right] \quad \text{E28}$$

$$\eta_{conc,\,CO} = \frac{RT_{ss}}{2F} ln\left[\left(\frac{x_{CO}^{bulk}}{x_{CO}^{TPB}}\right)\left(\frac{x_{CO_2}^{bulk}}{x_{CO_2}^{TPB}}\right)\right] \quad \text{E29}$$

The model used for the calculation of the gas species concentration at the TPB is reported in Campanari and Iora [11] according to the Dusty Gas Model previously described and under the conditions tested in this work, the resulting profiles will not be reported for sake of brevity. However, the corresponding set of equations is included in the model.

Activation overpotential

Activation overpotentials are associated to the energy needed to establish the two reactions of (i) hydrogen/carbon monoxide combination with oxygen ions and electrons and (ii) oxygen reduction, respectively at the anode and cathode layers. Activation overpotential losses are related to the current density throughout the Butler–Volmer equation, as listed in Table 4. The resulting correlations are reported in Table 6.

Table 6 – Correlations and values used for the calculation of activation overpotential losses in the model H_2-only and H_2–CO.

		Exchange current density and current density	Values
H_2-only from Aguiar et al. [10]	Cathode	$i_{0,cat} = \frac{RT}{n_eF}\, k_{cat} \cdot e^{\frac{-E_{cat}}{RT}}$ $i = i_{0,cat}\left[e^{\frac{n_e\eta_{act,cat}F}{RT}\alpha} - e^{\frac{n_e\eta_{act,cat}F}{RT}(\alpha-1)}\right]$	$k_{cat} = 2.35 \times 10^{11}\ \Omega\ m^{-2}$ $E_{cat} = 137 \times 10^3\ J\ mol^{-1}$ $\alpha = 0.5$
	Anode	$i_{0,an} = \frac{RT}{n_eF}\, k_{an} \cdot e^{\frac{-E_{an}}{RT}}$ $i = i_{0,an}\left[\frac{x_{H_2}^{TPB}}{x_{H_2}^{bulk}} e^{\frac{n_e\eta_{act,an}F}{RT}\alpha} - \frac{x_{H_2O}^{TPB}}{x_{H_2O}^{bulk}} e^{\frac{n_e\eta_{act,an}F}{RT}(\alpha-1)}\right]$	$k_{an} = 6.54 \times 10^{11}\Omega\ m^{-2}$ $E_{an} = 140 \times 10^3\ J\ mol^{-1}$ $\alpha = 0.5$
H_2–CO from Suwanwarangkul et al. [38]	Cathode	$i_{0,cat} = \left(\frac{p_{O_2}}{101325}\right)^{1/2} \frac{RT}{F}\, k_{cat} \cdot e^{\frac{-E_{cat}}{RT}}$ $i = i_{0,cat}\left[e^{\frac{-n_e\eta_{act,cat}F}{RT}} - e^{\frac{n_e\eta_{act,cat}F}{RT}}\right]$	$k_{cat} = 2.5 \times 10^9\ \Omega\ m^{-2}$ $E_{cat} = 130 \times 10^3\ J\ mol^{-1}$
	Anode H_2	$i_{0,H_2} = \left(\frac{p_{H_2,TPB}}{K_{eq,H_2} p_{H_2O,TPB}}\right)^{0.266} \frac{RT}{F}\, k_{an,H_2} \cdot e^{\frac{-E_{an,H_2}}{RT}}$	$k_{an,H2} = 2.1 \times 10^{11}\Omega\ m^{-2}$ $E_{an} = 120 \times 10^3\ J\ mol^{-1}$
	Anode CO	$i_{0,CO} = \left(\frac{p_{CO,TPB}}{K_{eq,H_2} p_{CO_2,TPB}}\right)^{0.266} \frac{RT}{F}\, k_{an,CO} \cdot e^{\frac{-E_{an,CO}}{RT}}$ $i_{H_2/CO} = i_{0,H_2/CO}\left[e^{\frac{n_e\eta_{act,an}F}{RT}} - e^{\frac{-\eta_{act,an}F}{RT}}\right]$	$K_{eq,H2} = \exp\left(\frac{29.5 \times 10^3}{T} - 6.41\right)$ $k_{an,CO} = 8.4 \times 10^{10}\Omega\ m^{-2}$ $E_{an,CO} = 120 \times 10^3\ J\ mol^{-1}$ $K_{eq,CO} = \exp\left(\frac{34.05 \times 10^3}{T} - 10.5\right)$

Thermal model

The solution of the electrochemical model equations is strongly influenced by the internal temperature profile. The energy balance equations are solved following a finite volume solution approach for each subsystem: the cathode and anode streams and the solid structure.

The energy balance of each cell element is calculated for the anode and the cathode sides with equations E30 and E31 respectively, taking into account the convective heat trans-fer between the solid parts and the flowing gases and considering the heat of reaction by means of the absolute enthalpies. The conductive thermal flux in the solid part of each element is modelled with the Fourier's law, by solving the energy balance equation E32. Radiative heat transfer is neglected for simplicity, provided that previous studies have shown that its effect generally does not imply significant changes in the overall energy balances, although influencing the solid structure temperature profiles [48]. The thermal model is described in details in Campanari and Iora [6].

$$\sum_{i}^{n} n_i^{in} h_i^{in} - \sum_{i}^{n} n_i^{out} h_i^{out} + \lambda_f A_f \left(T_{ss} - T_{f,bulk}\right) \qquad \text{E30}$$

where i = H_2, H_2O, CO, CO_2, CH_4, N_2

$$\sum_{i}^{n} n_i^{in} h_i^{in} - \sum_{i}^{n} n_i^{out} h_i^{out} + \lambda_a A_a (T_{ss} - T_{a,bulk}) \qquad \text{E31}$$

where i = O_2, N_2

$$\int_x \kappa_{ss} A_x \frac{\partial^2 T_{ss}}{\partial x^2} dx + \int_y \kappa_{ss} A_x \frac{\partial^2 T_{ss}}{\partial y^2} dy + \lambda_a A_a (T_{ss} - T_{a,bulk}) + \lambda_f A_f \left(T_{ss} - T_{fl,bulk}\right) + W_{el} + Q_{loss} = 0 \qquad \text{E32}$$

where W_{el} is the electric power and Q_{loss} is the thermal power dissipation.

Models comparison and analysis

The model implemented here (later labelled 'model' in diagrams and tables) has been compared with literature data and reference models (later labelled 'ref' in diagrams and tables) to evaluate the differences in cell performance predictions and in the profiles of relevant variables along the cell, thus allowing an additional validation. Depending on the type of literature data available, the comparison is carried out in the following sections with different types of fuel cells and different operating conditions, focusing case by case on specific aspects and model capabilities and trying to highlight their influence on the results.

Kinetic model comparison for HT SOFC operation and pressure effects

We first focus on the comparison of the kinetic model with a previous work based on HT-SOFC, comprehensively described in Campanari and Iora [6].

The purpose of this comparison is twofold: on one hand, to validate the new model with a previous one, validated at operating conditions typical HT-SOFCs. On the other hand, to highlight the influence of pressure on the models and their prediction of cell overall performance. In order to focus the present investigation only on the effects of the kinetic model, the electro-chemical model,[1] the cell geometry and the assumptions are taken equal to [6]. In particular, only H_2 oxidation is considered. The results of the comparison are reported in Table 7.

In terms of overall performance and gas composition at the anode/cathode outlet, the two models give the same results, allowing a mutual validation; also, the current densities profiles (which are not shown for brevity) and the total average current density closely match. Nevertheless, the gas concentration profiles differ, especially in pressurized operation, because the model adopted in Ref. [6] (whose kinetics is unaffected by the operating pressure) predicts a very high reaction rate of the SMR reaction, leading to a high H_2 concentration peak close to the entrance (Fig. 4). In case of the more refined kinetic model included here, CH_4 conversion is achieved more gradually and involves the central part of the cell too. The difference in the SMR reaction rate is also confirmed in the minimum solid temperature level, which is 14–15 °C higher. Finally, temperature profiles (not shown for brevity) are similar in the two cases, with differences mainly concentrated in first part of fuel channel, due to the different approach to SMR kinetics.

Comparison with a reference case at intermediate temperature (IT) and atmospheric pressure with pre-reformed NG

In this section the new model, selecting the option "H_2-only" has been compared with the results obtained in Aguiar et al. [10], where an IT-SOFC operating at atmo-spheric pressure is assessed. Pre-reformed natural gas is used as fuel. Reactants inlet temperature is set equal to 750 °C. The main data on the geometry of the fuel cell are reported in Table 5. The simulation is carried out by imposing the average current output and finding the cor-responding voltage: the cell is operated with a total current density of 5000 A/m^2 (according to the same analysis pro-posed in Ref. [10]) and the resulting electrochemical behaviour is presented in Fig. 5.

The model estimates a total cell voltage about 50–60 mV below (0.607 V vs. 0.67 V) the values predicted by Aguiar et al. [10]. The difference is not related to the prediction of overpotential losses, which are calculated with the same model and thus their average values ($\eta_{act,cat}$ 0.14 V, $\eta_{act,an}$ 0.087 V, η_{ohm} 0.051 V, η_{conc} 0.001 V) substantially agree with [10]. Conversely, the difference lies in the different evaluation of the Nernst potential, as highlighted by the term $\Delta E_{rev,H_2}$ in Fig. 5, whose average value is 0.056 V. The difference can be explained considering that the Nernst potential is affected by the H_2/H_2O concentration ratio along the cell, which is significantly different in this model because of the slower

[1] The electro-chemical model follows the approach proposed in Refs. [6,13,47] where the overpotential losses are calculated according with the equations proposed by the authors and shown in Table 4.

Table 7 – Preliminary validation for HT SOFC operation. Comparison at atmospheric and pressurized conditions of model and Ref. [6]. Common input parameters are: Syngas flow rate 0.51 mol/h CH_4 0.171, CO 0.294, H_2 0.263, H_2O 0.493,CO_2 0.044 (T 900 °C); Air flow rate 7.11 mol/h N_2 0.79, O_2 0.21 (T 900 °C); Cell with 18X18 channels, cell length 100 mm.

	Model	Ref. [6]	Δ%	Model	Ref. [6]	Δ%
	Atmospheric cell			Pressurized cell		
Anode outlet composition (% vol.)						
H_2	10.3	10.4	0.7%	11.6	11.5	−0.9%
H_2O	71.4	71.4	−0.1%	70.2	70.3	0.1%
CO	3.7	4.1	8.2%	3.7	3.9	6.2%
CO_2	14.4	14.1	−2.4%	14.5	14.3	−1.7%
CH_4	0.0	0.0		0.0	0.0	
Composition (% vol.)						
O_2	18.7	18.7	0.0%	18.8	18.8	0.0%
N_2	81.3	81.3	0.0%	81.2	81.2	0.0%
Main cell parameters						
Cell voltage, V	0.7	0.7	0.7	0.85	0.85	0.85
Net electric efficiency, %	50.9	50.5	−0.7%	60.6	60.4	−0.2%
DC power, W	15.1	15.0	−0.7%	17.9	17.9	−0.2%
Current density i, Am^{-2}	2150.4	2135.4	−0.7%	2107.5	2102.5	−0.2%
Fuel utilization factor U_f, %	80.7	80.1	−0.7%	79.0	78.9	−0.2%
Air utilization factor U_a, %	13.4	13.4	−0.7%	13.2	13.1	−0.2%
$T_{max,\ solid}$, °C	1009.1	1007.6	−0.1%	961.8	961.2	−0.1%
$T_{min\ solid}$, °C	868.3	854.9	−1.6%	854.5	840.5	−1.7%

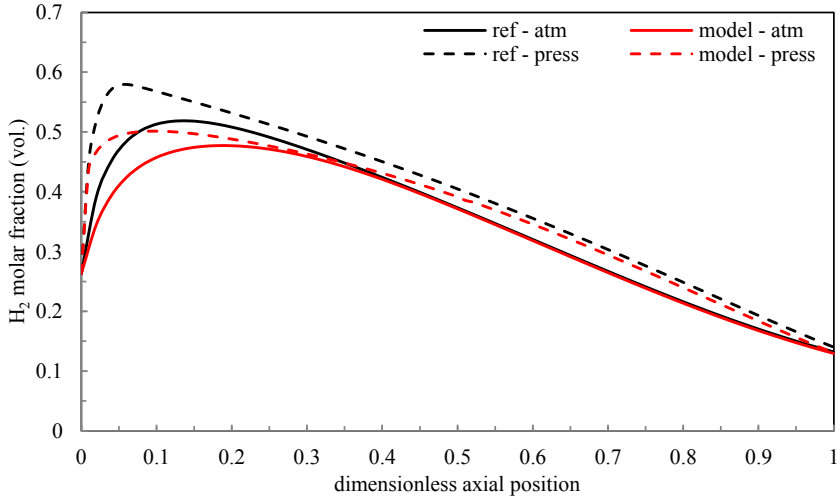

Fig. 4 – HT SOFC operation. H_2 molar fraction profiles prediction at atmospheric and pressurized conditions of the model and Ref. [6].

predicted CH_4 conversion. The average H_2/H_2O concentration ratio along the cell is equal to 0.3 vs. about 1.3 in Aguiar et al. [10], entailing a difference of the logarithmic term in the Nernst potential of about 0.056 V (assuming the average temperature of 800 °C). The fuel species concentration profiles along the cell are shown in Fig. 6.

Combined effect of H_2 and CO oxidation

The "H_2–CO" model have been compared with the numerical and experimental results presented from Suwanwarangkul et al. [38]. For a syngas composition of 40/60 of CO/H_2 diluted with 70% of N_2 working at 900 °C and 0.8 V the current density results of about 1100 A/m^2, which should be compared with the reference's value, 900 A/m^2. The difference can be explained by the following reasons: i) the design of our cell is slightly different than the cells used in their work, which is a button cell geometry; ii) the thermal model used in our system is not iso-thermal and therefore we have adapted the operating conditions in order to reach an almost constant cell temperature; iii) the material properties (thermal conductivity, resistivity, etc …) may slightly differ. Similar results have been obtained by comparing the syngas composition with 20/80 of CO/H_2.

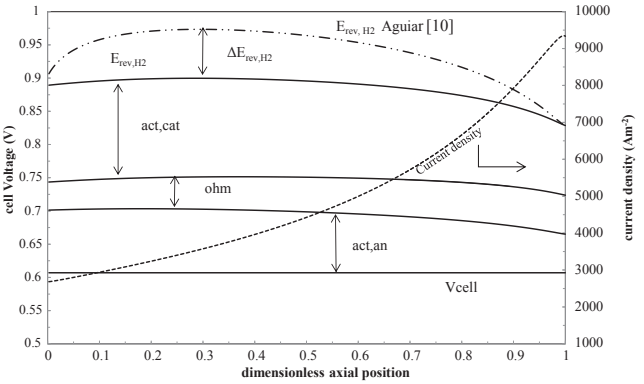

Fig. 5 – Case of atmospheric IT-SOFC with pre-reformed NG. Axial profiles of current density, Nernst potential and overpotential losses. The Nernst potential prediction in Aguiar et al. [10] is also reported.

The "H_2-only" and the "H_2–CO" model have been compared using three theoretical syngas compositions with different H_2/CO/N_2 ratio, namely, 20/0/80, 60/0/40, and 20/20/60 and operated both at atmospheric and pressurized conditions (20 bar). In case of "H_2–CO", an additional simulation has been performed for all the cases assuming the current density from CO equal to zero, in order to show the impact of CO oxidation mechanism within the same model. Such analysis is helpful to show the order of the error which would be expected if a SOFC model calibrated with a hydrogen based fuel (i.e. with no CO in the fuel and hence no CO-current considered – "H_2-only") was used when calculating the same cell operating with a CO-containing syngas.

Moreover, such cases are helpful to compare the two models with the same electrochemical oxidation mechanism, showing the differences that can be obtained with models calibrated on different fuel cells. As a matter of fact, different outputs are expected in this case from the two models due to the different equations and parameters used to compute the activation overpotentials (as shown in Table 6). Fuel and air inlet temperature has been set at 750 °C. A fuel utilization factor U_f of 70% has been fixed. An air utilization factor U_a of

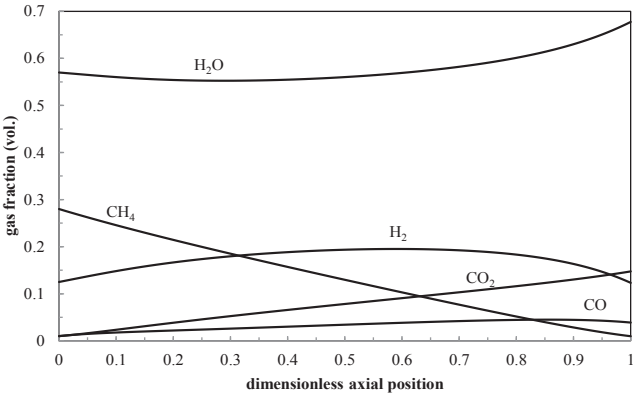

Fig. 6 – Case IT-SOFC with p_{atm} and pre-reformed NG. Fuel channel component molar fractions profiles (current density 5000 Am^{-2}).

3.3% has been assumed, resulting in an air flow rate limiting the maximum temperature rise in the fuel cell to less than 100 °C in all the cases examined. All the atmospheric cases have been calibrated to operate at 5000.0 A/m^2, whilst the pressurised ones at 10,000 A/m^2.

Results are shown in Fig. 7. It is worth noting that:

- The difference in the cell voltage prediction between the "H_2-only" and the "H_2–CO" model is remarkable (about 30%) at atmospheric pressure. The same cases run at 20 bar (not shown in figure) show a decrease of the voltage difference down to ~16%.
- When H_2 is used as fuel, the main differences between the two models are the activation losses at the anode and cathode sides. At the anode side, the "H_2–CO" model predicts a cell voltage drop almost double than in the "H_2-only" model (both for atmospheric and pressurized cases). At the cathode side, the "H_2–CO" model predicts 50% higher voltage losses at atmospheric pressure, reducing to almost no difference at pressurized conditions (not shown for brevity). This difference between atmospheric and pressurized cases at the cathode side is explained by the presence of O_2 partial pressure in the equation for the activation overpotential loss for the "H_2–CO" model.
- When CO is contained in the inlet feed, the "H_2–CO" model predicts a slightly higher cell voltage and higher Nernst voltage (associated to CO oxidation) compared to the previous cases with only H_2 feed; this rise, however, is compensated by the additional loss term related to the CO activation losses at the anode side. Hence, the relative difference between the two models remains at 26% and 16% for the atmospheric and the pressurised cases, respectively. In the conditions tested, the current density from H_2 oxidation (i_{H_2}) is always higher than the current density from CO oxidation (i_{CO}), representing about 60% and 70% of the total current at atmospheric and pressurized conditions respectively. Losses on the two branches of the model (see Fig. 1b) are represented in the last two cases of Fig. 7.
- Within the "H_2–CO" model approach, the voltage relative difference between the case with and without CO oxidation, when only H_2 is fed to the cell, is always negligible (<0.4%) at atmospheric pressure, whilst it becomes appreciable if pressurised operation is considered (≈2.5%). On the other hand, when CO is present in the anodic inlet stream (H_2/CO/N_2 = 20/20/60), the relative difference rises to 7.8% at atmospheric pressure and to 3% at 20 bar. It is therefore evident how the modeling error of neglecting the CO electrochemical oxidation is always appreciable, yet rather uncorrelated to the variation of inlet composition, in pressurised conditions, whilst it results extremely dependent on the fuel composition at atmospheric pressure.

In summary, we can conclude that the two models yield significantly different voltage predictions, also in the case of pure H_2 feed. Therefore, such differences appear as intrinsic to the fuel cell technology and type on which the parameters of the electrochemical model equations have been originally calibrated. However, if the CO oxidation influence is assessed

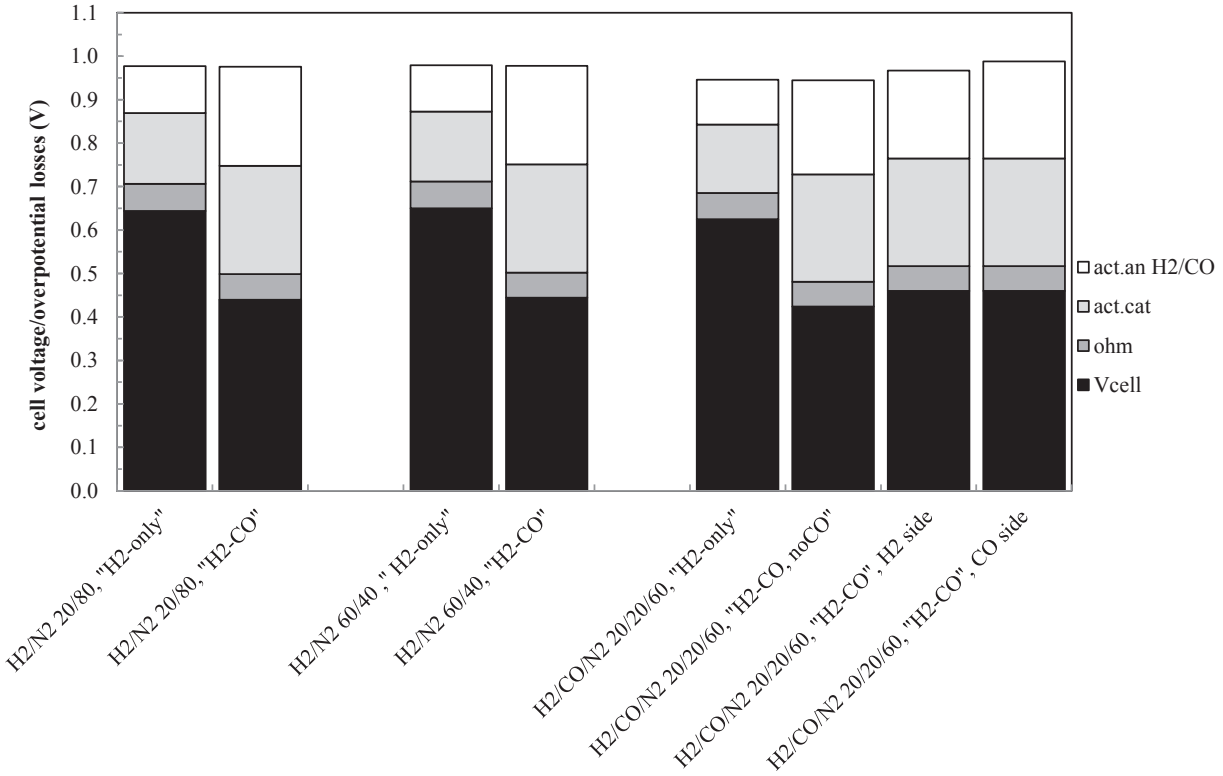

Fig. 7 – Comparison of "H_2-only"model and "H_2–CO" model using H_2-rich gas (with different H_2/CO/N_2 ratio) as fuel at atmospheric pressure and current density equal to 5000 Am^{-2}.

within the "H_2–CO" model, the voltage prediction is appreciable, yet not as much to considerably distort the overall performance prediction, especially in the pressurised case – as reported by some authors in the literature [37].

However, the H_2–CO model includes a more complete description of the process, since it takes into account the effect of the different components involved in the electrochemical conversion and the effect of pressure. Therefore, this latter model will be used in the following sections, where we consider different compositions of practical CO-rich syngas fuels.

Sensitivity analysis on syngas composition

A sensitivity analysis has been carried out on five representative syngas spanning over a variety of compositions, especially regarding the H_2 and CO molar fractions (Table 8). Such fuels are fed to a SOFC with current density of 2500, 5000 and 10,000 A/m^2 respectively for the atmospheric and the pressurized cases, with fuel utilization of 70% and air utilization of 3.3%.[2] The fuel flow rate has been varied in order to have the same equivalent hydrogen[3] to oxygen ratio ($H_{2,eq}/O_2$) at the fuel cell inlet in all the cases and a fixed air flow rate at the cathode side.

As shown in the previous section, the activation energy is highly dependent on the SOFC technology considered. Since the aim of this paper is not to assess a specific SOFC technology or material but to compare different modeling approaches, a sensitivity analysis on the activation energies has been performed. In particular, the activation energy has been reduced separately at the anode (for both H_2 and CO oxidation) and at the cathode side by 10% and 20% of the reference values. In addition, the H_2–CO *Evo* assumes a 20% combined reduction of the activation energies both at the anode and at the cathode sides.

In order to assess the effect of considering or not the direct CO oxidation, simulations have also been performed for all the cases by fixing a CO current density i_{CO} equal to zero.

The results in terms of cell voltage at the different operating conditions are presented in Table 9.

Syngas fuels with high CH_4 content (syngas A and C) feature the lowest cell voltages, mostly due to the lower H_2/CO content along the cell channels. This is mainly related to the steam reforming reaction rate which lowers the cell temperature level (the total temperature rise is about 55 °C for syngas A and C) compared to more than 70 °C for all the other cases with low methane content. Moreover, in those cases where CH_4 is converted with a slower kinetics (as discussed before), the decrease of H_2 and CO partial pressures decreases the Nernst voltage and therefore a lower cell voltage is obtained.

The implementation of CO oxidation in the model in-fluences the cell voltage prediction, especially for the high

[2] The sensitivity analysis is based on the comparison with respect to a reference case which, for each fuel composition considered, has been selected as the "H_2–CO" model calculated at 5000 A/m^2.

[3] $H_{2,eq} = H_2 + CO + 4CH_4$.

Table 8 – Gas composition of different syngas used for the sensitivity analysis.

[v/v]	Pre-reformed NG	Coal-based high-diluted	Coal syngas high CH_4	Biomass syngas	Coal-bases syngas
	Syngas A	Syngas B	Syngas C	Syngas D	Syngas E
N_2	0	0.02	0.15	0.4	0.01
H_2	0.26	0.06	0.2	0.17	0.15
H_2O	0.49	0.27	0.25	0.15	0.18
CO	0.03	0.2	0.04	0.13	0.33
CO_2	0.04	0.45	0.08	0.11	0.33
CH_4	0.18	–	0.28	0.04	–

Table 9 – Cell voltage prediction for different syngas at atmospheric and pressurized conditions resulting from the sensitivity analysis on the electrochemical model.

	Syngas A	Syngas B	Syngas C	Syngas D	Syngas E
	Pre-reformed NG	Coal-based high-diluted	Coal syngas high CH_4	Biomass syngas	Coal-bases syngas
Atmospheric pressure, $i = 5000$ A/m^2					
H_2–CO model	0.378	0.382	0.374	0.399	0.411
H_2–CO model, no CO	0.363	0.353	0.357	0.372	0.389
$E_{act\ an,\ H_2/CO}$ −10%	0.435	0.440	0.429	0.456	0.469
$E_{act\ an,\ H_2/CO}$ −20%	0.489	0.494	0.480	0.509	0.524
$E_{act\ cath}$ −10%	0.441	0.446	0.434	0.462	0.475
$E_{act\ cath}$ −20%	0.502	0.510	0.494	0.525	0.539
H_2–CO evo	0.612	0.622	0.596	0.636	0.652
H_2–CO evo, i 2500 A/m^2	0.708	0.705	0.708	0.720	0.734
High pressure (20 bar), $i = 10000$ A/m^2					
H_2–CO model	0.414	0.418	0.422	0.435	0.445
H_2–CO evo	0.646	0.654	0.653	0.669	0.681

CO content syngas (syngas B/D/E). In these cases, voltage differs by more than 5% between the cases with and without CO oxidation. The gas composition at the anode outlet shows a decrease in the CO content when both CO/H_2 currents are considered, due to the higher CO conversion (in case E, the CO molar fraction decreases from 11.2% to 10.6% when direct CO oxidation is included). Fig. 8 shows that, although the thermodynamic equilibrium of the shift reaction is almost the same in both cases (due to very similar temperature profiles), the WGS reaction rate profiles are greatly affected by the partial pressures of the reactants. When CO oxidation is activated, the amount of CO available for WGS, which

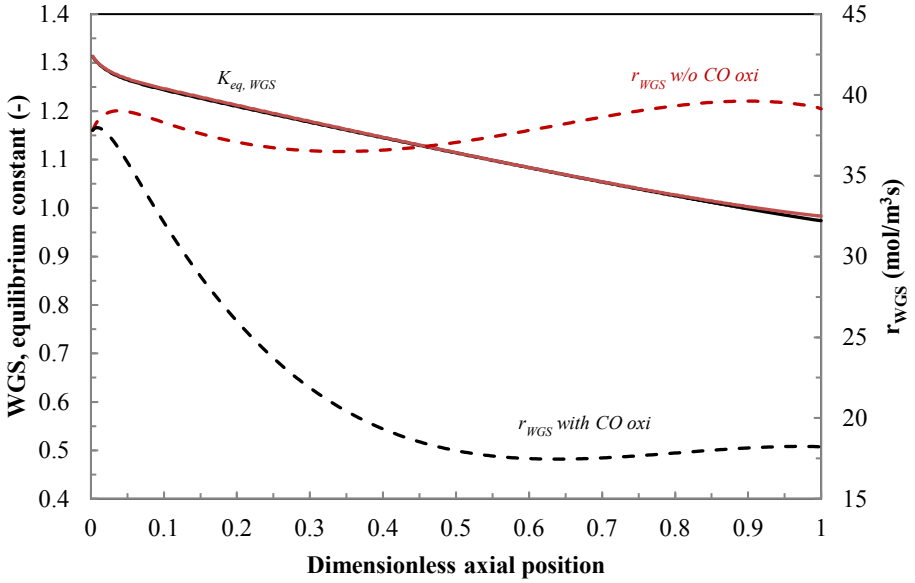

Fig. 8 – Effect of using CO oxidation mechanism in the electrochemical model on the WGS reaction equilibrium and the WGS reaction rate for syngas E.

competes with the electrochemical oxidation in terms of CO consumption, is lower compared to the case with only H_2 oxidation, thus reducing the WGS reaction rate.

Although a voltage variation is discernible, it is the authors' viewpoint that the described effect, between H_2-only and the H_2–CO cases, does not lead to grave misinterpretations of the overall cell performance. Therefore, it would be appropriate to consider more carefully the modeling trade-off between solution accuracy and numerical implementation. Surely, experimental analyses ought to be employed to shed additional light upon this issue.

When the activation energy is reduced by 10% and 20% with respect to the reference case, the cell voltage increases at the anode side by 15% and 29% respectively, without noticeable discrepancies between different syngas compositions. The same trend is detected when the activation energy decreases at the cathode side. In this case, the cell voltage increases by about 16% and 32%. In case of combined 20% reduction of cathode and anode activation energies, the voltage gain is approximately the sum of the two single contributions. As a matter of fact, the H_2–CO *Evo* configuration features a voltage increase which spans from about 59% to 63% and thus allows obtaining cell voltages which are of usual technological interest (>0.6 V).

The main consequence of the voltage gain can be observed from the interaction between the electrochemical model and the thermal model. An increased cell voltage, at the same fuel utilization (and air utilization), entails a larger portion of chemical energy converted into electricity. Therefore, less heat is generated at the electrodes and a lower temperature rise is observed along the cell (4–4.5 °C and 4.5–5 °C lower maximum temperature when decreasing the activation energy by 10% at the anode and at the cathode side respectively). Decreasing the activation energies (anode and cathode), the composition of the anode exhausts differs mostly in the higher CH_4 content (which is in the range of 3–4.5% for syngas A and 5–7% for syngas C), mostly due to the lower temperature in the cell. In fact, the higher the cell voltage, the lower the heat generated on the electrode and therefore the lower the temperature of the gases.

The importance of the CO electrochemical oxidation was also assessed in the *Evo* case with respect to the reference one; it has been found that the performance differences between the case with and without CO oxidation were comparable in the *Evo* and reference cases. Therefore, it shall be stated that the activation energy, and thus the cell voltage, does not contribute significantly to the importance of CO anodic oxidation.

When pressurized conditions are considered, the cell voltage gain is about 0.035–0.05 V for both the models used. In these cases, the higher pressure leads to higher Nernst voltages. On the other hand, the higher current density (10000 A/m^2) leads to almost double ohmic losses (e.g. 0.1 V at 20 bar compared to 0.056 V at atmospheric pressure for the reference case A).

The "H_2–CO evo" model has been tested also at lower current density (2500 A/m^2). Reducing the current density, the cell voltage gain spans from 0.082 V (case E) to 0.11 V (case C) with respect to the reference case (5000 A/m^2), mostly because of lower overpotential losses. In fact, ohmic resistance reduces by 0.027 V and cathode activation potential by 0.026 V. It is also important to notice that syngas A and C have the highest cell voltage increase (+0.10 and + 0.11 V respectively), because of a higher increase in the average Nernst potential both for H_2 and CO oxidation. The reason of this improvement is the CH_4 content in the anode exhaust gas, which decreases from 4.6% to 2.8% in syngas A whilst the final H_2 and CO content increases up to 10.6% and 1.7% (at 5000 A/m^2 the H_2/CO was respectively 5.1%/0.7%). As far as syngas C is concerned, CH_4 content decreases from 7.1% to 4.9% while H_2 and CO content at the outlet is respectively 7.6% and 2.4% (compared to 1.7% and 0.5% at 5000 A/m^2).

It has been observed that some syngas fuels show a reduction in CO current density with decreasing anodic E_act (i.e. syngas A and C) whilst others feature the opposite trend (i.e. syngas B, D and E). A wide-ranging analysis of the activation losses model (here not reported for brevity) evidences a correlation between the H_{2eq}/CO ratio, which characterises the inlet fuel composition and the reciprocal variation of H_2 and CO current densities at different activation energies. It turns out that syngas fuels with higher H_{2eq}/CO ratios (i.e. A and C) feature a rise of the H_2-related current density when the anode activation energy is reduced. On the other hand,

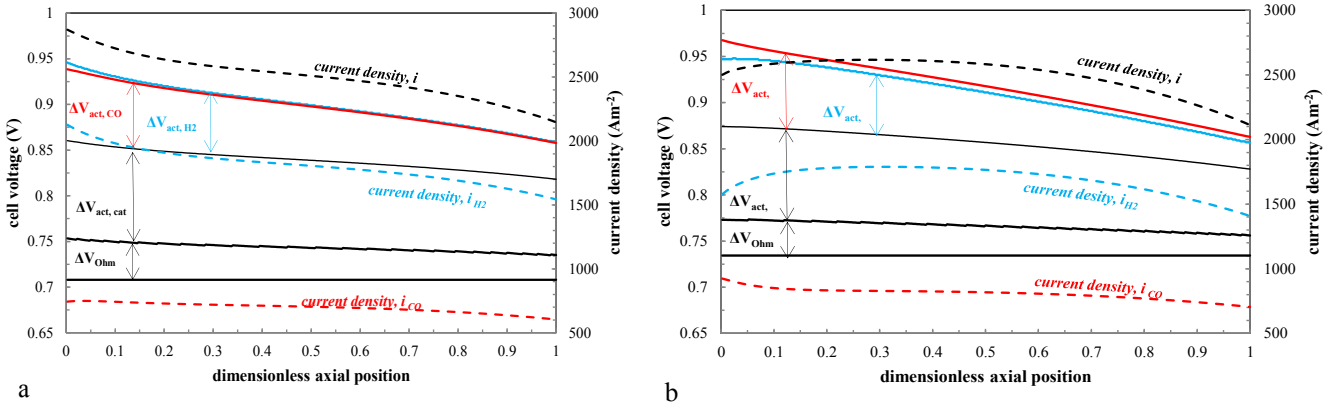

Fig. 9 – Overpotential losses profiles along the cell of syngas C (a) and syngas E (b) operated at atmospheric pressure using the "H_2–CO evo" model with 2500 A/m^2 of current density.

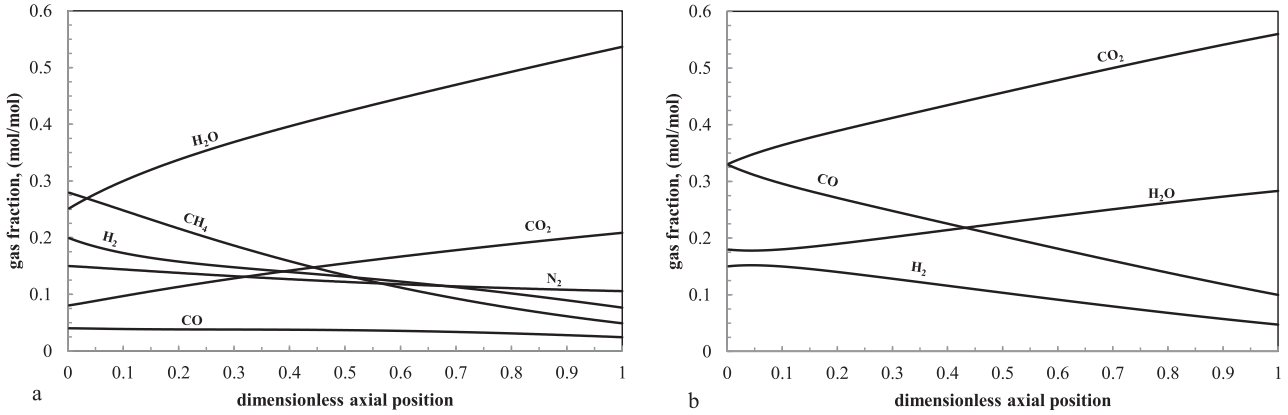

Fig. 10 – Gas fraction profiles along the anode side of the cell of syngas C (a) and syngas E (b) operated at atmospheric pressure using the "H_2–CO evo" model with 2500 A/m^2 of current density.

low H_{2eq}/CO values, which suggest a greater importance of carbon monoxide in the equivalent hydrogen overall production, are associated to a reduction of the H_2-related current density. This explains how the relative magnitude of H_2 and CO current density varies as a function of the inlet composition; therefore, models which fix a constant value of the exchange current densities i_{0H_2}/i_{0CO} (i.e. 2.5) should be carefully employed when dealing with syngas or hydrocarbon-based feeds.

In conclusion, the electrochemical behaviour of two representative cases (the coal-derived syngas E and CH_4-rich syngas C) operated at atmospheric pressure at 2500 A/m^2 are shown respectively in Fig. 9a and b. It is noteworthy that for syngas C, WGS reaction is close to the thermodynamic equilibrium along the cell since H_2 and CO have approximately the same chemical potential. On the other hand, syngas E features a H_2–CO Nernst potential difference of about 0.016 V and therefore the assumption of thermodynamic equilibrium would be less accurate.

The current density profiles are consistent with the gas composition profiles along the cell (Fig. 10a and b): with respect to case C, lower H_2 and CO concentrations are obtained along the cell because the CH_4 conversion by SMR reaction is not fast enough. Syngas E, on the other hand, is characterised by a slight rise in H_2 concentration at the channel inlet due to the effect of WGS reaction, leading to associated local current density increase.

SMR reaction rate effect

Reforming kinetics, influenced also by the choice of catalytic materials and their effectiveness, plays a central role in defining the cell temperature and concentration profiles and ultimately its performances. Considering the "H_2–CO Evo" model, an additional sensitivity analysis has been carried out about the methane reaction rate. Different anode materials, as well as catalyst load in the anode channel, can change the reaction rate of SMR, affecting in this way the gas composition and therefore the electro-chemical behav-iour and temperature profiles. Using a CH_4-rich syngas the SMR reaction rate has been varied from 0.5 to 20 times the value calculated by the reference model with equation (E10).

The resulting cell voltages are represented in Fig. 11, where it is possible to distinguish two different trends:

- at relatively low reaction rates (from 0.5 to 5 times the reference reaction rate), the cell voltage increases with the SMR conversion rate because the H_2/H_2O ratio and the CO content becomes higher, leading to a higher Nernst potential with a beneficial effect on the cell voltage.
- at higher reaction rates, the CH_4 conversion locally draws an increased thermal power, with negative consequences both in terms of cell temperature distribution and overpotential losses.

These opposite effects are connected to typical issues in the engineering and design of SOFCs with direct internal reforming, running with hydrocarbon-rich fuels:

- on one hand, the research activity on anode materials focuses on performing SMR with a reasonable reaction rate in

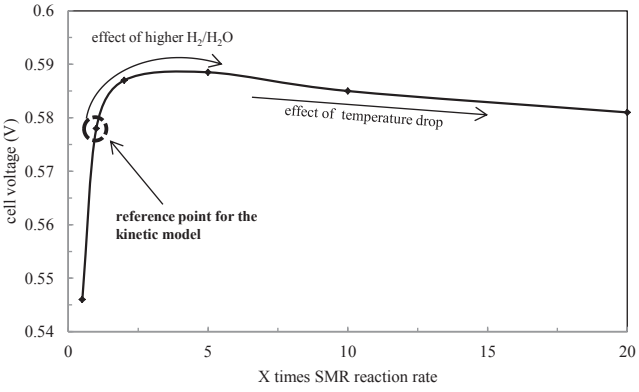

Fig. 11 – Cell voltage prediction of syngas (CH_4 30%, CO 10%, CO_2 4%, H_2 10%, H_2O 45%, N_2 1%) simulated with different SMR reaction rate velocities.

order to increase the H_2 production and thus the cell performance;

- on the other hand, it is often considered to add a pre-reforming step before the anode feed, to reduce the intensity of SMR reactions within the cell and convert higher hydrocarbons (such as n-butane, propane and ethane, etc.) into methane, H_2 and CO before entering the anode, reducing also the cell thermal gradients;
- with a similar purpose, some SOFC manufacturers are discussing about tailoring the SMR activity to reduce the thermal stresses brought about by the endothermic methane reforming reaction and preserve the SOFC lifetime. In this respect Boder et al. [49] proposed a wet impregnation procedure for modifying conventional cermets by coverage with a less active material (e.g. copper or iron) without compromising the electrochemical performance.

Effect of steam to-carbon (S/C) at different H_2/CO ratio Using high CO-rich syngas as feed gas for SOFC in power plants integrated with solid fuels gasification processes often penalizes the overall efficiency of the system due to the high steam consumption for syngas dilution for carbon deposition control.

In this section, the effect of the steam-to-carbon (S/C) on cell performance is studied by means of five fuels, characterised by different H_2/CO ratios ranging from 0.1 to 9, at three S/Cs values equal to 1, 2 and 3. These calculations have been performed considering a constant value of the air-to-fuel ratio for every employed fuel and keeping the molar flow rate of equivalent H_2 constant. In addition to this, the current density at which the cell operates has been increased up to 6000 A/m^2 compared to the previous cases in order to appreciate a greater effect of the CO oxidation contribution to the overall cell voltage.

The fuel cell voltage as a function of the H_2/CO and the steam to carbon ratio is shown in Fig. 12. It can be noticed that, by increasing the H_2/CO ratio, the cell voltage increases in all the cases due to the more pronounced effect of i_{H_2} compared to that of i_{CO}. An increased syngas dilution due to higher H_2O content decreases the cell voltage because a lower Nernst potential is obtained (which is directly correlated to the H_2/H_2O ratio). The cell voltage is always higher using both H_2 and CO oxidation mechanism as previously explained.

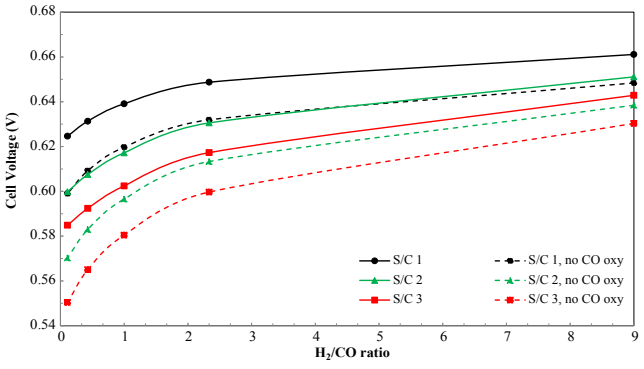

Fig. 12 – Cell voltage behaviour predicted by the "H_2–CO" model using syngas with different H_2/CO ratio and S/C. Dashed lines show the cell voltage behaviour of the system when the CO oxidation mechanism is not activated.

Carbon deposition

The model includes a qualitative analysis on the possibility to form solid carbon through the Boudouard and methane cracking reactions. Carbon deposition is an important issue to consider due to its implications on cell reliability and lifetime, other than on its electric efficiency.

The axial profile of the parameters α_{boud} and α_{crack} (equations E3 and E4) can be evaluated to check the possibility of carbon deposition along the cell length. Although these parameters do not allow the assessment of the quantity of solid carbon formed, which would need the implementation of a dedicated kinetic model, they would help, throughout a thermodynamic based method, to define those set of operating conditions, which would prevent the phenomena of carbon deposition from occurring. The α_j are function of pressure, temperature and gas concentration as they compare the actual gas composition with the chemical equilibrium constant of the reactions involved. It must be noticed that the Boudouard reaction is an exothermic reaction favoured at high pressure, while the methane cracking is an endothermic reaction favoured at low pres-sure. Therefore, they are favoured by opposite operating conditions.

The profiles of the abovementioned coefficients show that:

- At atmospheric pressure, α_{boud} is always higher than 10 and it increases along the cell due to the higher CO_2 concentration (and therefore the lower CO content). In case of methane cracking, the coefficient α_{crack} shows an opposite trend and it is always below 0.1 because of the low pressure, the increasing temperature, and the low CH_4 conversion associated to the low SMR reaction rate. Being α_{crack} lower than 1, methane cracking would proceed according to thermodynamics and a more advanced kinetic study would be needed to verify the safe operation of the fuel cell.
- At high pressure, both α_{boud} and α_{crack} are higher than 1 (except the α_{crack} for syngas C at the channel inlet due to the high CH_4 content). The main reason is related to the higher current density (10000 Am^{-2} compared to 5000 Am^{-2} at atmospheric pressure)
- As expected from the thermodynamic equilibrium analysis, at 20 bar, α_{boud} is significantly lower than at atmospheric conditions, while α_{crack} shows an opposite trend.
- At pressurized conditions both α_{boud} and α_{crack} increase along the cell. For syngas A and C (which have high CH_4 content), α_{boud} decreases at the channel inlet, due to the temperature drop associated to the steam reforming reaction. For the same reason, α_{crack} steeply increases in the same part of the cell.

The α_{boud} and α_{crack} profiles for the coal-derived syngas with high CH_4 content are shown in Fig. 13 as an example. The profiles obtained with the other fuels (not shown for

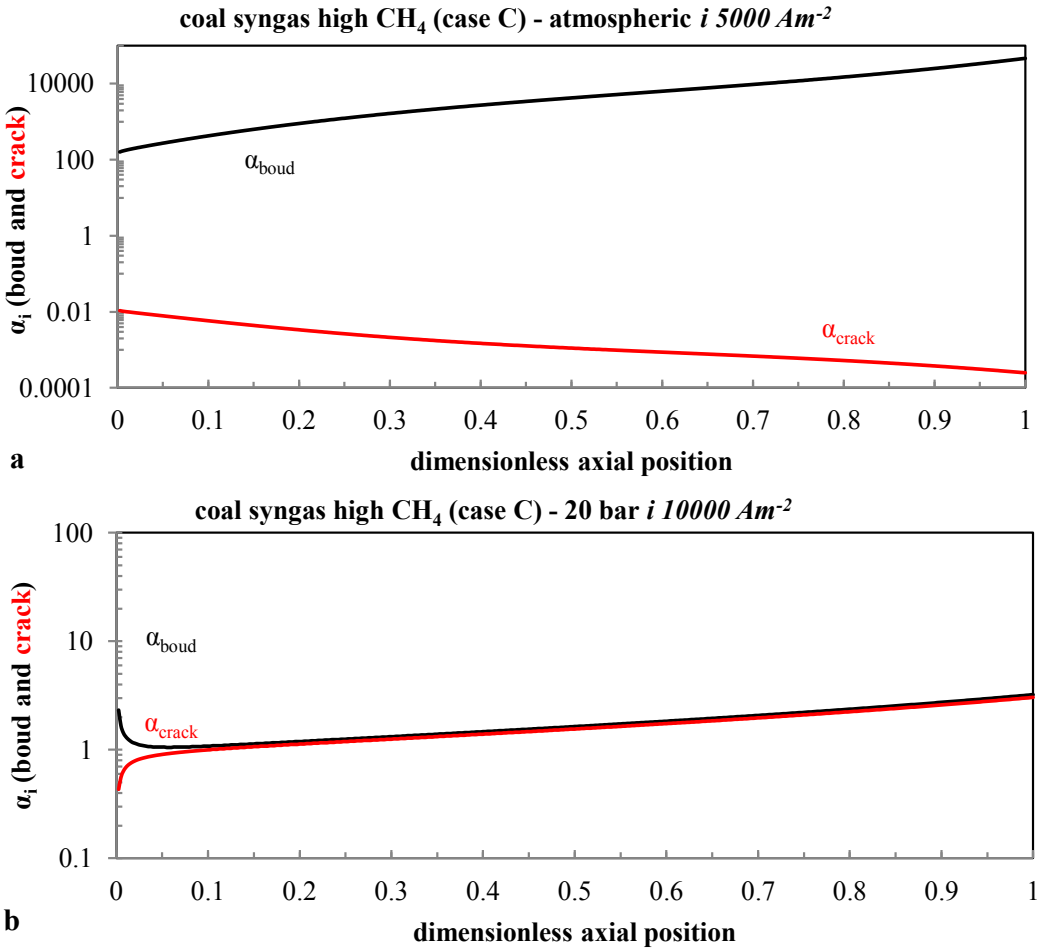

Fig. 13 – α_i profiles along the anode side of the cell for syngas C at different operating conditions.

brevity) have different absolute values but maintain the same trends.

Conclusions

This paper aims at shedding some light upon some delicate topics about SOFC modeling techniques, which are still shrouded by many uncertainties in the open literature. In particular, a thorough assessment of the impact on SOFC performance prediction of the effect of the combined electrochemical oxidation of CO and H_2 was sought. Moreover, this study proposes additional analyses to delve into the modeling of SMR and WGS kinetics. These aspects were developed as deeply correlated to the nature of the inlet fuel composition by studying SOFCs fed with syngas fuels such as those generated in coal-based or biomass gasification power plants. Such analysis has focused on the phenomenological SOFC modeling, where the results obtained are of direct interest for the design of integrated plant and for the related techno-economic assessments.

In order to reach this target, a previously developed model for SOFC simulation has been updated with new useful features, which comprise: (i) a kinetic representations of SMR and WGS reactions; (ii) detailed electrochemical models for either H_2-only or H_2–CO oxidation; (iii) evaluation of local carbon deposition risk according to Boudouard and methane cracking reactions. Validation of the relevant model parameters is based on a wide set of literature data that refers to both HT-SOFC and IT-SOFCs.

The first notable result is that models which have been calibrated for H_2-only oxidation and those which considers both H_2 and CO oxidation are characterised by remarkable voltage prediction differences (approximately 30%) both with only H_2 feed and with H_2/CO mixture feed.

However, if the CO electrochemical oxidation impact was to be assessed only within a "H_2–CO" model (switching on and off the CO-related current density), its effect on the overall performance, for high CO content syngas fuels, drops to values around 7% and 3%, at atmospheric pressure and pressurised conditions respectively. These results question the idea that CO electrochemical oxidation might radically distort the performance prediction of SOFCs.

A sensitivity analysis has been performed on the activation energy at both anode and cathode electrodes in order to enhance the voltage levels predicted by the "H_2–CO" model to values comparable to those of technological interest nowadays. This led to the development of an enhanced

H_2–CO electrochemical model obtained with the definition of a set of appropriate parameters to be applied in the subsequent analysis of different syngas fuels. Results of the simulations confirm the capability of the enhanced H_2–CO model to better take into account the effect of various H_2/CO ratios in the syngas fuel on the cell performances, compared to the H_2-only electrochemical model. The analysis also scoped the impact of CO oxidation at different activation energies, and thus voltages, showing that little contribution is expected for all the fuel compositions considered.

A conclusive remark upon the H_2–CO combined oxidation shows the existence of a correlation between the relative proportion of H_2 and CO-related current densities magnitudes and a parameter representing the inlet fuel composition, H_{2eq}/CO. It has been found that higher this parameter gets, the greater the importance of H_2 current density is upon that of CO. This should drive the attention towards those models present in the literature, which are based on a constant a ratio between i_{0H_2} and i_{0CO}; these should in fact be applied with caution when dealing with extremely different syngas compositions.

In conclusion, a sensitivity analysis on the SMR reaction rate was performed pointing out the presence of a maximum value of the cell voltage at relatively low reaction rates; this results has also been justified by the recent trends in terms of reforming catalyst material research.

Appendix

In this section is reported the demonstration of the statement that in presence of WGS reaction at the chemical equilibrium, the Nernst voltage of H_2 oxidation and CO oxidation reactions are the same. If WGS reaction is at the chemical equilibrium condition, it is possible to write:

$$K_{EQ\ wgs} = \exp\left(-\frac{\Delta G^0_{WGS}}{RT}\right) = \frac{\left(p_{CO_2} p_{H_2}\right)}{\left(p_{CO} p_{H_2O}\right)}$$

If the Gibbs free energy of the WGS reaction is decomposed and the term $(G^0_{02})^{0.5}$ is added and subtracted, after some mathematical steps is possible to distinguish the Gibbs free energy of CO oxidation and H_2 oxidation as follows:

$$\exp\left(-\frac{\left(\Delta G^0_{CO,\,OX} - \Delta G^0_{H_2,OX}\right)}{RT}\right) = \frac{\left(p_{CO_2} p_{H_2}\right)}{\left(p_{CO} p_{H_2O}\right)} \rightarrow \frac{\exp\left(-\frac{\left(\Delta G^0_{CO,\,OX}\right)}{RT}\right)}{\exp\left(-\frac{\left(\Delta G^0_{H_2,OX}\right)}{RT}\right)} = \frac{\left(p_{CO_2} p_{H_2}\right)}{\left(p_{CO} p_{H_2O}\right)}$$

If the ratio of products/reactants partial pressure is multiplied and divided to the square root of O_2 partial pressure, rearranging the equation and considering the logarithm properties:

$$ln\left(\frac{\left(p_{CO}\left(p_{O_2}\right)^{0.5}\right)}{\left(p_{CO_2}\right)}\right) + \left(-\frac{\left(\Delta G^0_{CO,\,OX}\right)}{RT}\right) = ln\left(\frac{\left(p_{H_2}\left(p_{O_2}\right)^{0.5}\right)}{\left(p_{H_2O}\right)}\right) + \left(-\frac{\left(\Delta G^0_{H_2,OX}\right)}{RT}\right)$$

If both terms are multiplied for the term $\frac{RT}{2F}$, we have:

$$-\frac{\left(\Delta G^0_{CO,\,OX}\right)}{2F} - \frac{RT}{2F} ln\left(\frac{\left(p_{CO_2}\right)}{\left(p_{CO_2}\right)\left(p_{CO}\left(p_{O2}\right)^{0.5}\right)}\right) = -\frac{\left(\Delta G^0_{H_2,\,OX}\right)}{2F} - \frac{RT}{2F} ln\left(\frac{\left(p_{H_2O}\right)}{\left(p_{H_2}\left(p_{O_2}\right)^{0.5}\right)}\right)$$

and the equation above corresponds to the equivalence of Nernst voltage for the CO and the H_2 oxidation reactions, i.e. $E_{rev,CO} = E_{rev,H_2}$.

REFERENCES

[1] Veyo SE, Shockling LA, Dederer JT, Gillett JE, Lundberg WL. Tubular solid oxide fuel cell/gas turbine hybrid cycle power systems: status. J Eng Gas Turbines Power 2002;124:845–9.

[2] Liese E. Comparison of preanode and postanode carbon dioxide separation for IGFC systems. J Eng Gas Turbines Power 2010;132:061703.

[3] Verma A, Rao AD, Samuelsen GS. Sensitivity analysis of a vision 21 coal based zero emission power plant. J Power Sources 2006;158:417–27.

[4] Vora SD, Energy S. SECA program review. In: Ninth Annu SECA Work Pittsburgh, PA; 2006.

[5] Zhao Y, Sadhukhan J, Lanzini A, Brandon N, Shah N. Optimal integration strategies for a syngas fuelled SOFC and gas turbine hybrid. J Power Sources 2011;196:9516–27.

[6] Campanari S, Iora P. Comparison of finite volume SOFC models for the simulation of a planar cell geometry. Fuel Cells 2005;5:34–51.

[7] Romano MC, Campanari S, Spallina V, Lozza G. Thermodynamic analysis and optimization of it-SOFC-based integrated coal gasification fuel cell power plants. J Fuel Cell Sci Technol 2011;8:041002.

[8] Li M, Rao AD, Brouwer J, Samuelsen GS. Design of highly efficient coal-based integrated gasification fuel cell power plants. J Power Sources 2010;195:5707–18.

[9] Romano MC, Spallina V, Campanari S. Integrating IT-SOFC and gasification combined cycle with methanation reactor and hydrogen firing for near zero-emission power generation from coal. Energy Procedia 2011;4:1168–75.

[10] Aguiar P, Adjiman CS, Brandon NP. Anode-supported intermediate temperature direct internal reforming solid oxide fuel cell. I: model-based steady-state performance. J Power Sources 2004;138:120–36.

[11] Campanari S, Iora P. Definition and sensitivity analysis of a finite volume SOFC model for a tubular cell geometry. J Power Sources 2004;132:113–26.

[12] Achenbach E, Riensche E. Methane/steam reforming kinetics for solid oxide fuel cells. J Power Sources 1994;52:283–8.

[13] Costamagna P, Selimovic A, Del Borghi M, Agnew G. Electrochemical model of the integrated planar solid oxide fuel cell (IP-SOFC). Chem Eng J 2004;102:61–9.
[14] Li M, Powers JD, Brouwer J. A finite volume SOFC model for coal-based integrated gasification fuel cell systems analysis. J Fuel Cell Sci Technol 2010;7:041017.
[15] Gemmen RS, Trembly J. On the mechanisms and behavior of coal syngas transport and reaction within the anode of a solid oxide fuel cell. J Power Sources 2006;161:1084–95.
[16] Lehnert W, Meusinger J, Thom F. Modelling of gas transport phenomena in SOFC anodes. J Power Sources 2000;87:57–63.
[17] Haberman BA, Young JB. Three-dimensional simulation of chemically reacting gas flows in the porous support structure of an integrated-planar solid oxide fuel cell. Int J Heat Mass Transf 2004;47:3617–29.
[18] Divisek J, de Haart L, Holtappels P. The kinetics of electrochemical reactions on high temperature fuel cell electrodes. J Power Sources 1994;49:257–70.
[19] Yakabe H, Ogiwara T, Hishinuma M, Yasuda I. 3-D model calculation for planar SOFC. J Power Sources 2001;102:16–25.
[20] Janardhanan VM, Deutschmann O. CFD analysis of a solid oxide fuel cell with internal reforming: coupled interactions of transport, heterogeneous catalysis and electrochemical processes. J Power Sources 2006;162:1192–202.
[21] Hecht ES, Gupta GK, Zhu H, Dean AM, Kee RJ, Maier L, et al. Methane reforming kinetics within a Ni-YSZ SOFC anode support. Appl Catal A Gen 2005;295:40–51.
[22] Hofmann P, Panopoulos KD, Fryda LE, Kakaras E. Comparison between two methane reforming models applied to a quasi-two-dimensional planar solid oxide fuel cell model. Energy 2009;34:2151–7.
[23] Andersson M, Yuan J, Sundén B. Review on modeling development for multiscale chemical reactions coupled transport phenomena in solid oxide fuel cells. Appl Energy 2010;87:1461–76.
[24] Mogensen D, Grunwaldt JD, Hendriksen PV, Dam-Johansen K, Nielsen JU. Internal steam reforming in solid oxide fuel cells: status and opportunities of kinetic studies and their impact on modelling. J Power Sources 2011;196:25–38.
[25] Miao H, Wang WG, Li TS, Chen T, Sun SS, Xu C. Effects of coal syngas major compositions on Ni/YSZ anode-supported solid oxide fuel cells. J Power Sources 2010;195:2230–5.
[26] Klein J-M, Bultel Y, Pons M, Ozil P. Modeling of a solid oxide fuel cell fueled by methane: analysis of carbon deposition. J Fuel Cell Sci Technol 2007;4:425.
[27] Bedogni S, Campanari S, Iora P, Montelatici L, Silva P. Experimental analysis and modeling for a circular-planar type IT-SOFC. J Power Sources 2007;171:617–25.
[28] He W, Zou J, Wang B, Vilayurganapathy S, Zhou M, Lin X, et al. Gas transport in porous electrodes of solid oxide fuel cells: a review on diffusion and diffusivity measurement. J Power Sources 2013;237:64–73.
[29] Chan S, Khor K, Xia Z. A complete polarization model of a solid oxide fuel cell and its sensitivity to the change of cell component thickness. J Power Sources 2001;93:130–40.
[30] Suwanwarangkul R, Croiset E, Fowler MW, Douglas PL, Entchev E. Douglas M a. Performance comparison of Fick's, dusty-gas and Stefan–Maxwell models to predict the concentration overpotential of a SOFC anode. J Power Sources 2003;122:9–18.
[31] Yakabe H, Hishinuma M, Uratani M, Matsuzaki Y, Yasuda I. Evaluation and modeling of performance of anode-supported solid oxide fuel cell. J Power Sources 2000;86:423–31.
[32] Noren DA, Hoffman MA. Clarifying the Butler–Volmer equation and related approximations for calculating activation losses in solid oxide fuel cell models. J Power Sources 2005;152:175–81.
[33] Achenbach E. Three-dimensional and time-dependent simulation of a planar solid oxide fuel cell stack. J Power Sources 1994;49:333–48.
[34] Nishino T, Iwai H, Suzuki K. Comprehensive numerical modeling and analysis of a cell-based indirect internal reforming tubular SOFC. J Fuel Cell Sci Technol 2006;3:33.
[35] Petruzzi L, Cocchi S, Fineschi F. A global thermo-electrochemical model for SOFC systems design and engineering. J Power Sources 2003;118:96–107.
[36] Matsuzaki Y, Yasuda I. Electrochemical oxidation of H_2 and CO in a H_2-H_2O-CO-CO_2 system at the interface of a Ni-YSZ cermet electrode and YSZ Electrolyte. J Electrochem Soc 2000;147:1630.
[37] Ni M. Modeling of SOFC running on partially pre-reformed gas mixture. Int J Hydrogen Energy 2012;37:1731–45.
[38] Suwanwarangkul R, Croiset E, Entchev E, Charojrochkul S, Pritzker MD, Fowler MW, et al. Experimental and modeling study of solid oxide fuel cell operating with syngas fuel. J Power Sources 2006;161:308–22.
[39] Andersson M, Yuan J, Sundén B. SOFC modeling considering hydrogen and carbon monoxide as electrochemical reactants. J Power Sources 2013;232:42–54.
[40] Iwai H, Yamamoto Y, Saito M, Yoshida H. Numerical simulation of intermediate-temperature direct-internal-reforming planar solid oxide fuel cell. Energy 2011;36:2225–34.
[41] Park J, Li P, Bae J. Analysis of chemical, electrochemical reactions and thermo-fluid flow in methane-feed internal reforming SOFCs: part II-temperature effect. Int J Hydrogen Energy 2012;37:8532–55.
[42] Razbani O, Assadi M, Andersson M. Three dimensional CFD modeling and experimental validation of an electrolyte supported solid oxide fuel cell fed with methane-free biogas. Int J Hydrogen Energy 2013;38:10068–80.
[43] Schluckner C, Subotić V, Lawlor V, Hochenauer C. Three-dimensional numerical and experimental investigation of an industrial-sized SOFC fueled by diesel reformat – Part II: detailed reforming chemistry and carbon deposition analysis. Int J Hydrogen Energy 2015;40:10943–59.
[44] Schluckner C, Subotić V, Lawlor V, Hochenauer C. Three-dimensional numerical and experimental investigation of an industrial-sized SOFC fueled by diesel reformat – Part I: creation of a base model for further carbon deposition modeling. Int J Hydrogen Energy 2014;39:19102–18.
[45] Hajimolana SA, Hussain MA, Daud WMAW, Soroush M, Shamiri A. Mathematical modeling of solid oxide fuel cells: a review. Renew Sustain Energy Rev 2011;15:1893–917.
[46] Kakaç S, Pramuanjaroenkij A, Zhou XY. A review of numerical modeling of solid oxide fuel cells. Int J Hydrogen Energy 2007;32:761–86.
[47] Iora P, Campanari S. Development of a three-dimensional molten carbonate fuel cell model and application hvbrid cycle simulations. J Fuel Cell Sci Technol 2007;4:501–10.
[48] Iora P, Campanari S. Effect of radiation in circular-planar type it-SOFCs operating in stack configuration. In: Eur. SOFC Forum, Luzern; 2008.
[49] Boder M, Dittmeyer R. Catalytic modification of conventional SOFC anodes with a view to reducing their activity for direct internal reforming of natural gas. J Power Sources 2006;155:13–22.